Space Sci Rev (2007) 129: 207–243
DOI 10.1007/s11214-007-9192-4

A Comparative Study of the Influence of the Active Young Sun on the Early Atmospheres of Earth, Venus, and Mars

Yuri N. Kulikov · Helmut Lammer · Herbert I.M. Lichtenegger · Thomas Penz · Doris Breuer · Tilman Spohn · Rickard Lundin · Helfried K. Biernat

Received: 1 February 2006 / Accepted: 10 April 2007 /
Published online: 8 June 2007

Abstract Because the solar radiation and particle environment plays a major role in all atmospheric processes such as ionization, dissociation, heating of the upper atmospheres, and thermal and non-thermal atmospheric loss processes, the long-time evolution of planetary atmospheres and their water inventories can only be understood within the context of the evolving Sun. We compare the effect of solar induced X-ray and EUV (XUV) heating on the upper atmospheres of Earth, Venus and Mars since the time when the Sun arrived at the Zero-Age-Main-Sequence (ZAMS) about 4.6 Gyr ago. We apply a diffusive-gravitational equilibrium and thermal balance model for studying heating of the early thermospheres by photodissociation and ionization processes, due to exothermic chemical reactions and cooling by IR-radiating molecules like CO_2, NO, OH, etc. Our model simulations result in extended thermospheres for early Earth, Venus and Mars. The exospheric temperatures obtained for all the three planets during this time period lead to diffusion-limited hydrodynamic escape of atomic hydrogen and high Jeans' escape rates for heavier species like H_2, He, C, N, O, etc. The duration of this blow-off phase for atomic hydrogen depends essentially on the mixing ratios of CO_2, N_2 and H_2O in the atmospheres and could last from ∼100 to several hundred million years. Furthermore, we study the efficiency of various non-thermal atmospheric loss processes on Venus and Mars and investigate the possible protecting effect of the early martian magnetosphere against solar wind induced ion pick up

Yu.N. Kulikov (✉)
Polar Geophysical Institute (PGI), Russian Academy of Sciences, Khalturina Str. 15, 183010 Murmansk, Russian Federation
e-mail: kulikov@pgi.ru

H. Lammer · H.I.M. Lichtenegger · T. Penz · H.K. Biernat
Space Research Institute, Austrian Academy of Sciences, Schmiedlstr. 6, 8042 Graz, Austria

D. Breuer · T. Spohn
Institute of Planetary Research, German Aerospace Center, Rutherfordstr. 2, 12489 Berlin, Germany

R. Lundin
Swedish Institute of Space Physics (IRF), P.O. Box 812, 98128 Kiruna, Sweden

erosion. We find that the early martian magnetic field could decrease the ion-related non-thermal escape rates by a great amount. It is possible that non-magnetized early Mars could have lost its whole atmosphere due to the combined effect of its extended upper atmosphere and a dense solar wind plasma flow of the young Sun during about 200 Myr after the Sun arrived at the ZAMS. Depending on the solar wind parameters, our model simulations for early Venus show that ion pick up by strong solar wind from a non-magnetized planet could erode up to an equivalent amount of ∼250 bar of O^+ ions during the first several hundred million years. This accumulated loss corresponds to an equivalent mass of ∼1 terrestrial ocean (TO (1 TO $\sim 1.39 \times 10^{24}$ g or expressed as partial pressure, about 265 bar, which corresponds to ∼2900 m average depth)). Finally, we discuss and compare our findings with the results of preceding studies.

Keywords Early atmospheres · Atmospheric evolution · Thermospheric heating · Solar induced atmospheric loss

1 Introduction

As discussed by Lundin et al. (2007, this issue) solar radiation and particle fluxes play a major role in all atmospheric processes. So, the evolution of planetary atmospheres can only be understood within the context of the evolving Sun. The escape of atmospheric constituents from the upper planetary atmospheres depends on the evolution of the solar X-ray and EUV (XUV) radiation ($\lambda \leq 102.7$ nm), which affects dissociation and ionization processes; the thermosphere and exosphere temperatures; and thermal and non-thermal escape rates. Observations and studies of isotope anomalies in planetary atmospheres (e.g., Lammer et al. 2000a; Lammer and Bauer 2003; Becker et al. 2003; and references therein), radiative fluxes, stellar magnetic fields, stellar winds of solar-type stars with different ages (Zahnle and Walker 1982; Sonnett et al. 1991; Ayres 1997; Guinan and Ribas 2002; Wood et al. 2002, 2005; Ribas et al. 2005; Lundin et al. 2007, this issue), and lunar and meteorite fossil records (Newkirk 1980) indicate that the young Sun underwent a highly active phase after the formation of the Solar System, which lasted about 0.5–1.0 Gyr and included frequent flare events where the particle flux and radiation intensity were several hundred times more intense than today.

Recent astrophysical multiwavelength (X-ray, EUV, FUV, UV, optical) observations of solar-type stars (solar proxies) with ages which cover most of the Sun's main sequence lifetime from 0.13–8.5 Gyr (carried out within the *Sun in Time* program (Dorren and Guinan 1994; Guinan and Ribas 2002; Ribas et al. 2005) and discussed in Lundin et al. (2007, this issue)) indicate that the coronal XUV emissions of the young main-sequence Sun were about 100 to 1000 times stronger than those of the Sun today. Thus the age-radiation relationship of the solar proxies indicates that the XUV flux of the young Sun at about 2.5 Gyr, 3.5 Gyr and 4.5 Gyr ago was about 3, 6 and 100 times higher, respectively, than today (Ribas et al. 2005), which is in general agreement with the previous studies by Iben (1965), Cohen and Kuhi (1979), Gough (1977), Zahnle and Walker (1982), Sonnett et al. (1991), and Ayres (1997), although these studies focused on stars that are not "real" solar proxies.

Besides solar radiation, the solar wind plasma flux is another important factor related to the evolution of planetary atmospheres because it induces non-thermal ion loss from weakly or non-magnetized planetary atmospheres. Recent Hubble Space Telescope high-resolution

spectroscopic observations of the H Lyman-α feature of several nearby main-sequence stars carried out by Wood et al. (2002, 2005) have revealed neutral hydrogen absorption associated with the interaction between the stars' fully ionized coronal wind with the partially ionized local interstellar medium. Wood et al. (2002, 2005) modelled the absorption features formed in the astrospheres of these stars and provided the first empirically-estimated coronal mass loss rates for G-K main sequence stars (see also Lundin et al. 2007, this issue). It was found that the correlation between mass loss and the X-ray surface flux of young solar-like stars obeys a power law relationship, which indicates an average solar wind density up to 1000 times higher than today during the first 100 Myr after the Sun reached the Zero-Age-Main-Sequence (ZAMS).

However, recent observations by Wood et al. (2005) of the absorption signature of the astrosphere of the ∼0.55 Gyr old solar-like star, ξ Boo, indicate that there may possibly exist a high-activity cutoff regarding the stellar mass loss in a radiation-activity-relation derived in the form of a power law by Wood et al. (2002). They also find that the mass loss of that particular star is about 20 times less than the average stellar mass loss value inferred at about 4 Gyr. As pointed out by Ribas et al. (2005), Wood et al. (2005) and Lundin et al. (2007, this issue), more measurements would be needed to define better the mass loss and activity relation for "cool" main sequence stars, especially at high activity levels.

The aim of the present work is to apply thermospheric balance and diffusive equilibrium models to study the effect of the evolving solar XUV radiation and solar wind plasma on the early upper atmospheres of Earth, Venus and Mars in a comparative way. In Sect. 2, we discuss the heating of the Earth's thermosphere by ionizing radiation. We apply a thermospheric model to the present Earth atmosphere and vary the mixing ratio of CO_2, NO molecules, etc., which act as thermospheric coolers due to their IR emission. In Sect. 3, we apply our models to early Earth, Venus and Mars and study the thermospheric heating and exospheric temperatures as a function of neutral gas composition and solar XUV radiation. In Sect. 4, we discuss the impact of non-thermal atmospheric loss processes over the history of Venus and Mars and the atmospheric protection effect for the early martian atmosphere by the martian magnetic dynamo. Finally, we discuss in Sect. 5 the results of our study and implications for the early atmospheric evolution of Venus, Earth and Mars and their water inventories.

2 Thermospheric Heat Balance and Composition Modelling

The main radiation responsible for heating of upper atmospheres and the formation of planetary ionospheres is the solar XUV radiation. The part of the atmosphere where the XUV radiation is absorbed and a substantial fraction of its energy is transformed into heat, leading to a positive temperature gradient $dT/dz > 0$, is the thermosphere, which extends from about 90 to 210 km on Venus and Mars and from about 90 to 500 km on Earth.

In the lower thermosphere convection can play an important role in the transport of heat, while in the upper thermosphere heat is transported by molecular conduction, leading to an isothermal region ($T = \text{const}$). In the part of the atmosphere which is called the exosphere, where the mean free path of the atmospheric species is large and collisions become negligible, lighter atmospheric constituents whose thermal velocity exceeds the gravitational escape velocity, can escape from the planet. The base of the exosphere is defined as an altitude level where the mean free path is about equal to the local scale height $H = kT_{\text{exo}}/mg$ of the gas, with k the Boltzmann constant, T_{exo} the temperature at the exobase, g the gravitational acceleration, and m the mass of the main atmospheric species. The exobase level on Venus and Mars is located at an altitude of about 210 km and on Earth at about 500 km.

The most important heating and cooling processes in the upper atmosphere of Earth can be summarized as follows (e.g., Izakov 1971; Dickinson 1972; Chandra and Sinha 1974; Gridchin et al. 1975; Gordiets et al. 1978, 1979; Gordiets and Kulikov 1981, 1982; Gordiets et al. 1982, 1987; Gordiets 1991; Dickinson et al. 1987):

1) heating due to CO_2, N_2, O_2, and O photoionization by the solar XUV radiation ($\lambda \leq$ 102.7 nm),
2) heating due to O_2 and O_3 photodissociation by the solar UV radiation,
3) chemical heating in exothermic binary and 3-body reactions,
4) neutral gas molecular heat conduction,
5) turbulent energy dissipation and heat conduction,
6) heating and cooling due to contraction and expansion of the thermosphere,
7) IR-cooling in the vibrational-rotational bands of CO_2, NO, O_3, OH, NO^+, $^{14}N^{15}N$, CO, etc.

Gordiets et al. (1979, 1981, 1982), Gordiets and Kulikov (1981) applied a numerical model to calculate the thermal budget of the Earth's thermosphere in the altitude range of 90–500 km. Their model includes the main energy sources and sinks, such as IR-radiative cooling in the vibrational-rotational bands of optically active molecules, as well as heating and cooling arising from dissipation of turbulent energy and eddy heat transport. The heating by the solar XUV radiation of the present Earth's thermosphere yields an average exospheric temperature of ~1000 K (e.g., Jacchia 1977; Crowley 1991). The results of their simulations which are in agreement with observations, revealed that the most efficient heat source in the Earth's thermosphere is due to photoionization by the XUV radiation and heating which arises from photodissociation of O_2 (e.g., Gordiets et al. 1982; Hunten 1993). These thermospheric heating processes are balanced by the main cooling processes which include IR radiative cooling in the 1.27–63 μm wavelength range and cooling due to molecular and eddy conduction (e.g., Gordiets et al. 1982).

In the present study we apply a thermospheric model based on the models of Gordiets et al. (1982) and Gordiets and Kulikov (1985) to the terrestrial, venusian, and martian atmospheres by considering the expected evolution of the solar XUV flux from 100 XUV about 4.5 Gyr ago to 1 XUV (present time normalized solar value). The thermospheric models solve in the vertical direction the 1-D time-dependent equations of continuity and diffusion for nine atmospheric constituents (CO_2, O, CO, N_2, O_2, Ar, He, NO, and H_2O), hydrostatic and heat balance equations, and the equations of vibrational kinetics for radiating molecules from below the base of the thermosphere (mesopause), up to the exobase. The model is self-consistent with respect to the neutral gas temperature and vibrational temperatures of the minor species radiating in the IR. It takes into account heating due to the CO_2, N_2, O_2, CO, and O photoionization by the XUV-radiation ($\lambda \leq$ 102.7 nm), heating due to O_2 and O_3 photodissociation by solar UV-radiation, chemical heating in exothermic 3-body reactions, neutral gas molecular heat conduction, IR-cooling in the vibrational-rotational bands of CO_2 (15 μm), CO, O_3, and in the 63 μm O line, and turbulent energy dissipation and heat conduction. We use the volume heating and cooling rates for the processes included in our simulations and the heating rates owing to photodissociation which are discussed in detail by Gordiets et al. (1978, 1979, 1982) and Gordiets and Kulikov (1981, 1982, 1985). The lower boundary conditions for the system of 1-D time-dependent hydrodynamic equations modelling the termosphere are

$$\rho = \rho_0, \qquad T = T_0, \tag{1}$$

where T is the temperature, ρ the gas density and T_0 and ρ_0 are taken from available observational data. The upper boundary of the model is at the exobase level where one can assume

$$\frac{\partial T}{\partial z} = 0, \qquad \frac{\partial^2 v_z}{\partial z^2} = 0, \tag{2}$$

here v_z is the vertical bulk gas velocity of the atmosphere.

The thermospheres of the terrestrial planets are heated mainly, as was noted above, by the absorption of the solar X-ray and extreme ultraviolet (EUV) radiation. In photoionization most of the excess solar photon energy is carried away by the electrons produced. These photoelectrons may cause secondary and further ionization, dissociation and excitation of electronic states of molecules and atoms. In photodissociation the excess energy can go into internal energy of the products, or it may be released as kinetic energy. To calculate the thermospheric heating rate due to the solar XUV radiation, it is conventional to introduce into heat balance models the "solar heating efficiency", which is the fraction of the solar energy absorbed that appears locally as heat. Among many other authors, notably Torr et al. (1979, 1980), Fox and Dalgarno (1981) and Fox (1988) have contributed to the present understanding of this key parameter for the terrestrial planets.

For the Earth's thermosphere it is now generally agreed that the heating efficiency has its maximum of 50–55% of the absorbed radiative energy at the heights of about 150–180 km, while below this altitude, where the solar heating is dominated by the Schumann–Runge continuum photodissociation, its value decreases to about 30%. Above ~300 km where heating in chemical reactions becomes less important due to decreasing atmospheric collision rates, the heating efficiency also decreases down to values of about 10% (see, for example, Torr et al. 1980). Since most of the solar energy is deposited at heights below 200 km, it seems reasonable, in view of many uncertainties in the model parameters, to use for our heat balance calculations a height-averaged value of ~50% for the heating efficiency in the Earth's thermosphere.

Fox and Dalgarno (1981) and later Fox (1988) calculated the EUV heating efficiencies in the thermosphere of Venus for different assumptions about the fraction of excess energy converted to vibrational excitation in elementary molecular processes. In their model Fox and Dalgarno (1981) assumed that half of the excess energy released in photodissociation of CO_2 and in chemical reactions produces vibrational excitation of the molecular products. Calculated altitude-dependent heating efficiencies were around 18% below 130 km and 22% above 135 km. The lower and upper limits according to their estimates were 10% and 30%, approximately. A later more strict analysis by Fox (1988) constrained the heating efficiency between about 22% in the lower region (below ~130 km) and 25% in the upper region of the day time thermosphere of Venus. However, our estimated heating efficiencies for the present time thermospheres of Venus and Mars of about 16% and 8%, correspondingly, appear to be considerably smaller than the values obtained by Fox (1988). This problem with the heating efficiency in a CO_2 atmosphere is not new, however, and has been also encountered in the modelling works of other authors (Dickinson and Bougher 1986; Hollenbach et al. 1985). More dedicated studies are needed in the future to resolve this discrepancy.

IR emission of CO_2 in the 15 μm band is the major cooling process in the lower thermospheres of Venus, Earth and Mars (e.g., Gordiets et al. 1982; Gordiets and Kulikov 1985; Bougher et al. 1999; Bougher et al. 2000). For the calculation of the heat loss rate q_{CO_2} due to IR emission of CO_2 in the 15 μm fundamental band excitation of the $CO_2(01^\circ 0)$ bending mode vibration-rotation states in collisions with heavy particles like atomic oxygen and CO_2, N_2, etc., collisional radiative de-excitation processes and absorption of radiation

are taken into account. For the 15 μm CO_2-band we use the "cool-to-space" approximation (e.g., Dickinson 1972; Gordiets et al. 1982) which can be expressed as

$$q_{CO_2} = 1.33 \times 10^{-13} g_w e^{-960/T} n_{CO_2} \left(\sum_M k_M n_M \right) F(\tau, \xi), \tag{3}$$

where $g_w = 2$ is a statistical weight factor for the 01°0 CO_2 molecule states, k_M is the relaxation rate constant for collisions with molecules and atoms having density n_M (CO_2, O, O_2, N_2, etc.), n_{CO_2} is the CO_2 number density and $F(\tau, \xi)$ accounts for the absorption of radiation in the band (Gordiets et al. 1982). Here τ is the reduced optical depths of the atmosphere for the 15 μm radiation at the height in question, ξ is the ratio of the radiative to the net relaxation rate of the 01°0 CO_2 states at the same height.

The eddy conduction heating rate q_{ec} can be calculated by

$$q_{ec} = \frac{\partial}{\partial z} \left[\rho c_p K_{eh} \left(\frac{\partial T}{\partial z} + \frac{g}{c_p} \right) \right], \tag{4}$$

where K_{eh} is the eddy heat conductivity assumed to be equal to the eddy diffusion coefficient and c_p is the specific heat at constant pressure. Because of a stable thermospheric stratification

$$\frac{\partial T}{\partial z} + \frac{g}{c_p} > 0, \tag{5}$$

the vertical heat flux owing to eddy conduction is always negative and directed downward to the mesosphere. Therefore, the net effect of eddy conduction is thermospheric cooling. One should note that locally at some level eddy conduction may either heat or cool the thermosphere, depending on the value of $\partial(\rho K_{eh})/\partial z$ (Gordiets et al. 1982). Furthermore, we also include in our model simulations heating due to dissipation of turbulent energy

$$q_{eh} = q_d + q_g, \tag{6}$$

where q_d and q_g are the volume rates of turbulent energy dissipation owing to the action of viscous and buoyancy forces

$$q_d = K_{eh} \frac{\rho g}{T} \left(\frac{\partial T}{\partial z} + \frac{g}{c_p} \right) \frac{1 - R_{dyn}}{R_{dyn}}, \tag{7}$$

and

$$q_g = K_{eh} \frac{\rho g}{T} \left(\frac{\partial T}{\partial z} + \frac{g}{c_p} \right). \tag{8}$$

Here R_{dyn} is the dynamic Richardson number for the statistically steady turbulent motion which can be expressed as

$$R_{dyn} = \frac{\varepsilon_g}{\varepsilon_s} = \frac{\frac{K_{eh} g}{K_{em} T} \left(\frac{\partial T}{\partial z} + \frac{g}{c_p} \right)}{\left(\frac{\partial u}{\partial z} \right)^2} = \alpha_t Ri, \tag{9}$$

where ε_s is the transfer rate of kinetic energy from the mean motion to fluctuation motion and can be written as

$$\varepsilon_s = K_{em} \left(\frac{\partial u}{\partial z} \right)^2, \tag{10}$$

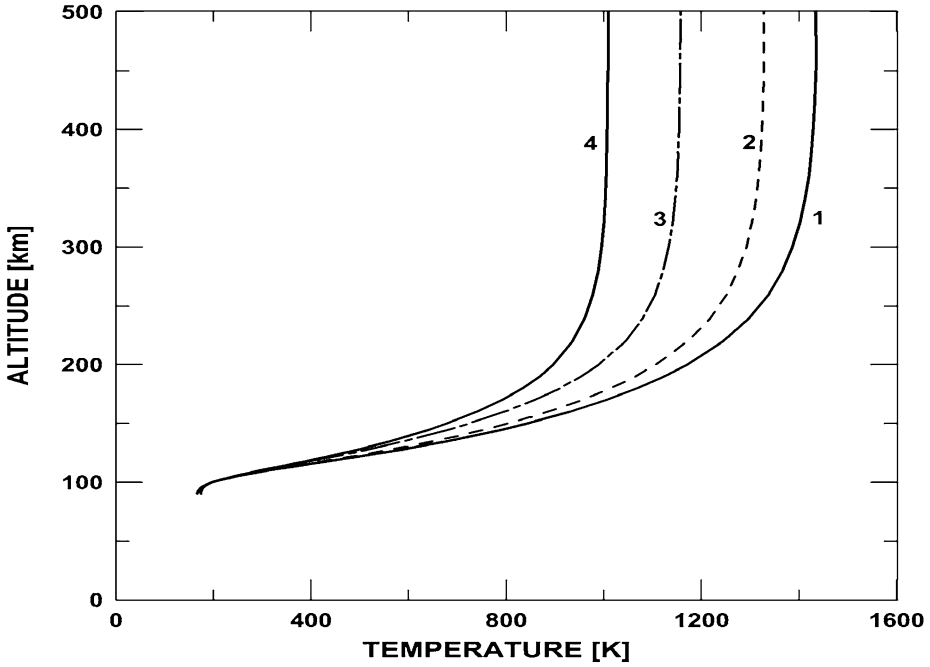

Fig. 1 Temperature of the present time Earth thermosphere showing the effect of various IR-radiating molecules on the temperature profiles. (*1*) Only 15 μm CO_2 fundamental band is cooling; (*2*) Cooling by O 63 μm IR-line plus CO_2 cooling; (*3*) NO cooling in the 5.3 μm fundamental band plus O and CO_2 cooling; (*4*) All the previously mentioned coolers including chemically excited IR bands of minor molecular constituents and cooling in the OH 2.8 μm, O_3 in 9.6 μm, and $O_2(^1\Delta_g)$ 1.27 μm bands are taken into account

with K_{em} the eddy momentum diffusion coefficient, Ri the usual Richardson number and u the horizontal component of the mean velocity of motion. The value of ε_g is the net amount of the potential gas energy associated with buoyancy forces and α_t is the reciprocal of the turbulent Prandtl number (Gordiets et al. 1982).

From the above brief description of our thermospheric models used in this study their major intrinsic limitations can be summarized as follows: 1) the present stage models do not incorporate the upper atmospheric photochemistry of CO_2, H_2O, O_2, etc.; 2) the models do not include hydrogen loss, neither Jeans nor hydrodynamic, thus they should be applied only to the upper atmospheres which are not hydrogen-rich or humid. Therefore, the major uncertainties of our simulations which are closely related to the above model limitations, can result in considerable underestimation of the thermospheric cooling due to intensive atomic hydrogen hydrodynamic loss from a "wet" terrestrial thermosphere at high exobase temperatures, especially at temperatures above the critical value for blow off. The obtained exospheric temperatures should be considered as an approximate upper limit to real thermospheric temperatures. The uncertainties associated with the absence of detailed photochemical calculations in the models may lead to systematically increasing errors in the assumed solar XUV heating efficiency for high XUV fluxes as the flux grows and, therefore, may result in substantial exobase temperature errors during the young Sun period. Also, there are uncertainties in the IR-cooling rates calculation from hot and expanded terrestrial thermospheres, as well as some others which seem, however, to be less important. Therefore, more work is in progress which will advance these thermospheric models to a higher

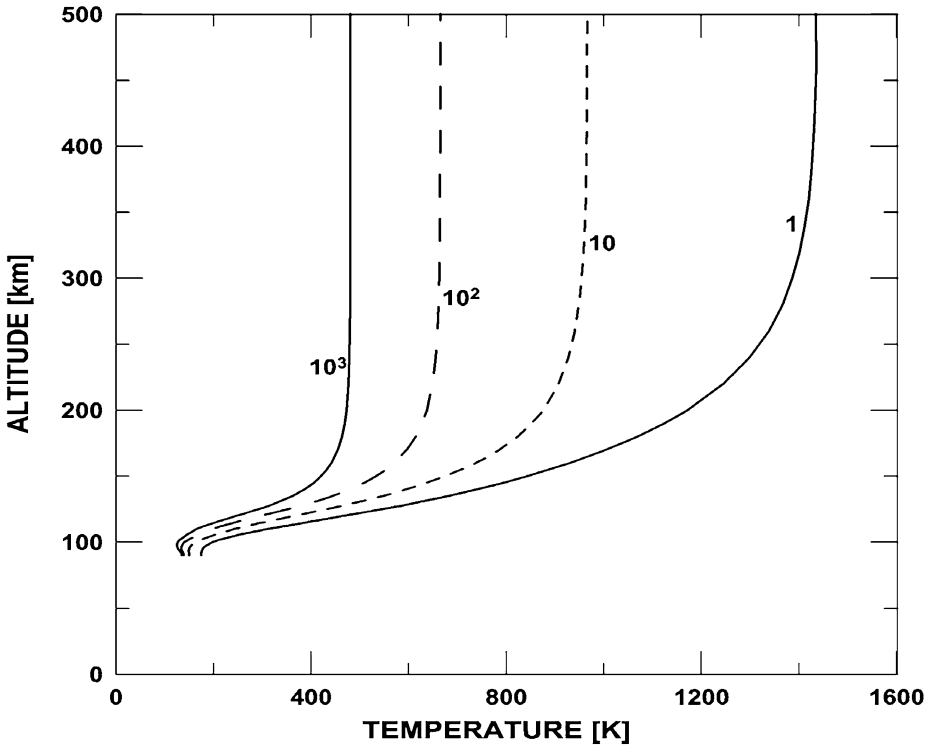

Fig. 2 Thermospheric temperature profiles for present time Earth with different CO_2 mixing ratios. The mixing ratios are expressed in units of PAL—Present Atmospheric Level: 1 PAL $= 3.3 \times 10^{-4}$ of the CO_2 mixing ratio

level of fidelity. However, one should note that hydrodynamic outflow conditions and effective planetary hydrogen winds depending on the available H_2O reservoirs and climate conditions may last for relatively short time periods during the planet's evolutionary stage, resulting in much "dryer" or less humid atmospheres, such as those considered in the present study.

Figure 1 shows the effect of various IR-irradiating molecules on the temperature profile of the present upper atmosphere of Earth. Figure 2 shows the effect of various CO_2 mixing ratios on the Earth's thermospheric temperature profile. One can see that a mixing ratio which is $\geq 10^3$ times higher than that of the present Earth would produce an exospheric temperature which is slightly larger than the present value for Venus (see Fig. 5 for comparison). It should be noted that the temperature profiles presented in Fig. 2 are calculated for an atmosphere containing only CO_2 as an IR-radiating molecule. All the other IR-cooling species shown in Fig. 1 are not included in the model calculations shown in Fig. 2. One can see from Figs. 1 and 2, that CO_2 can be the most efficient cooler due to IR emission in the 15 μm fundamental band for the terrestrial planetary atmospheres.

Since we are interested in the effect of higher XUV flux values produced by the young Sun (see Ribas et al. 2005; Lundin et al. 2007, this issue) on the upper atmospheres of the early terrestrial planets, we calculate in Sects. 3.1, 3.2 and 3.3 the thermospheric temperature and density profiles for early Earth, Venus and Mars.

3 Comparative Study of the Evolution of the Upper Atmospheres of Terrestrial Planets

3.1 Early Earth

For a study of the heating of the Earth thermosphere by XUV radiation from the young Sun, we apply our thermospheric model to an atmosphere with the present atmospheric composition and a related heating efficiency for the solar XUV radiation. The heating efficiency of the ionizing solar radiation in the terrestrial thermosphere can be estimated through the analysis of the photoelectron and ion energy production processes and the ways of conversion of the non-thermal energy of the photolysis products into heat. As it is known, about 50% of 34 eV, which is the average energy of a solar ionizing quantum, is spent for ion production, while the other half is carried away by primary photoelectrons which are able to produce further ionizations, gas particle excitations, etc. The photoionization and following it neutralizing ionospheric chemical reactions in the terrestrial thermosphere result in the formation of two O atoms per each ionization act which takes away from local gas heating the dissociation energy of the O_2 molecule. This energy is carried down from the thermosphere by a diffusion flux of oxygen atoms which recombine only near the base of the thermosphere or below. Also, a part of the energy released in the ionospheric chemical reactions goes into "pumping" of the internal energy levels of the atomic, ion, and molecular reaction products. A part of this internal energy can be radiated away to space in the UV, visible, and infra-red spectral ranges and thus be lost, while the other part, due to particle collisions, is thermalized and heats the ambient gas. The estimations by Gordiets et al. (1979) for the terrestrial oxygen-rich thermosphere resulted in an average value of about 50%, which is used in the present study.

All the IR-cooling mechanisms of the model are included in these calculations. Figure 3 shows the calculated exospheric temperature related to the solar XUV flux as a function of time. As shown by Ribas et al. (2005) and Lundin et al. (2007, this issue), the solar XUV flux was ~6 times higher 3.5 Gyr ago, ~10 times higher 3.8 Gyr ago, ~50 times higher 4.33 Gyr ago, and reached ~100 times the present Sun level ~4.5 Gyr ago. One can see from Fig. 3, that the blow-off temperature for atomic hydrogen of about 5000 K would be exceeded during the first Gyr after the Sun arrived at the ZAMS, or before 3.5 Gyr ago. Here we assume that when the thermal energy of gas-kinetic motion exceeds its gravitational energy, the top of the atmosphere blows off and moves radially away from the planet (Öpik 1963). The critical temperature for the start of the blow off is then given by

$$T_c = \frac{2M_{pl}mG}{3kr}. \tag{11}$$

Here M_{pl} is the planetary mass, m the mass of atomic hydrogen, G Newton's gravitational constant, and r is the planetocentric distance of the exobase. For the XUV fluxes more than 10 times the present flux (>3.8 Gyr ago) on Earth one would expect very high exospheric temperatures that could result in large thermal escape rates even for heavier species like H_2, He, N, O, and C. However, we should note that the calculated, extremely high exobase temperatures (T_{exo} ~ 10000–20000 K) being much above the blow off temperature for hydrogen, should be considered as rather rough estimates of the expected upper limits for T_{exo}, because of the intrinsic limitations and uncertainties of our model thermospheres, as discussed in the previous section.

Figure 4 shows the effect of the solar XUV radiation on the early Earth's exobase temperature for different levels of the CO_2 mixing ratio at the base of the thermosphere. For

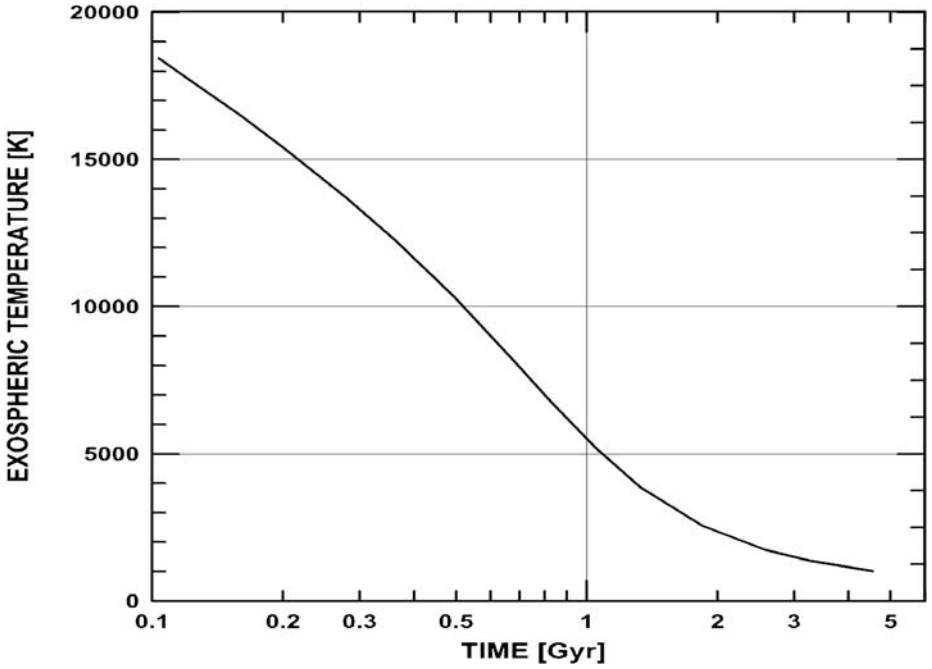

Fig. 3 Time evolution of the exospheric temperature based on Earth's present atmospheric composition over the planets' history as a function of the solar XUV flux for a strongly limited hydrogen blow-off rate

simulations with the CO_2 mixing ratios higher than its present atmospheric level (1 PAL), both the total number density at the lower boundary, which is located at the base of the thermosphere (∼90 km), as well as the ratio of the N_2 to O_2 number densities have been kept constant. The ratio N_2/O_2 has been assumed to be equal to its present time value of ∼3.7. The atmospheric levels of Ar and He have been kept at 1 PAL. It should be noted that only the 15 μm CO_2 cooling is included in these calculations to show clearly its effect on the exobase temperature.

As can be seen from Fig. 4, a low CO_2 level implies higher exobase temperatures and an increased atmospheric loss when compared with high CO_2 abundance. Therefore, in the case of a low CO_2 level a higher loss rate of hydrogen and water vapor from the Earth's atmosphere can be expected over longer periods of time, up to about 1 Gyr, or even longer. As a result, early Earth could have lost a large amount of water if it were not protected by a strong magnetic field, due to both thermal and non-thermal escape. Atmospheric levels of CO_2 higher than in the present Earth's atmosphere, inferred from paleosols—soil samples around 2.2–2.75 Gyr ago (e.g., Raye et al. 1995; Hessler et al. 2004), would thus imply lower exobase temperatures and a reduced loss as compared to an early atmosphere with a present atmospheric level of CO_2. However, we cannot say anything definite about the CO_2 level in the ancient Earth atmosphere at this stage of research.

In their recent study Tian et al. (2005, 2006) apply a 1-D time-dependent hydrodynamic escape model to simulate thermal escape processes from a molecular hydrogen-rich early Earth's atmosphere. Because the solar XUV radiation levels were much stronger during the Archean era than today, they adopt XUV radiation levels of 1, 2.5, and 5 times the present value in their simulations. These authors also assume high CO_2 mixing ratios in the early

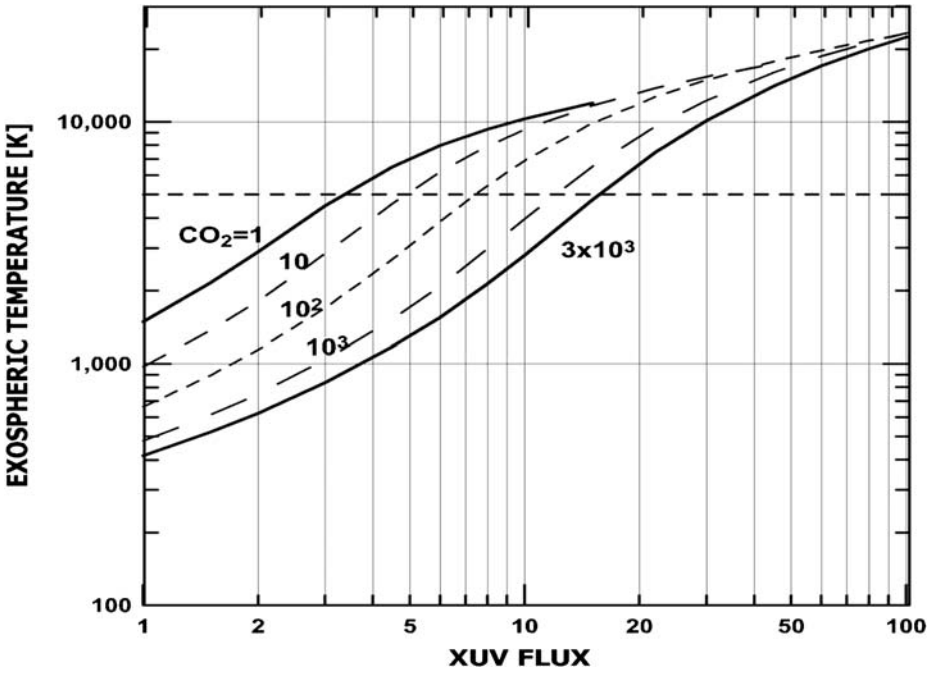

Fig. 4 Earth's exospheric temperatures for different levels of CO_2 abundance in units of PAL in the thermosphere as a function of solar XUV flux. The *numbers by the curves* correspond to CO_2 volume mixing ratios expressed in PAL (Present Atmospheric Level: 1 PAL for $CO_2 = 3.3 \times 10^{-4}$). The *horizontal dashed line* shows the blow-off temperature of atomic hydrogen

Earth's atmosphere but do not actually include IR-cooling by CO_2 in the energy balance equation of their model and argue that low oxygen and high CO_2 on early Earth yielded a cold exobase.

Applying their model, Tian et al. (2005) calculate the temperature and velocity profiles for the corresponding XUV radiation levels and obtain very low temperatures at the exobase of early Earth's atmosphere in the range of ∼300–600 K due to the adiabatic cooling associated with hydrodynamic escape. Although the flow velocity near the upper boundary of their model for all the three cases considered is below the escape velocity from the planet, they conclude that even in the 1 XUV level case hydrodynamic escape of molecular hydrogen would still occur. Tian et al. (2005) also calculate the hydrodynamic and Jeans escape rates for varying hydrogen homopause mixing ratios resulting from their simulations[1]. Jeans escape rates found by Tian et al. (2005) are more than one order of magnitude smaller than their simulated hydrodynamic escape rates due to the low exobase temperatures.

However, their hydrodynamic blow off solutions for an H_2-rich early Earth atmosphere at the extremely low exobase temperatures of 300–600 K are in disagreement with the predictions of the classical Jeans kinetic loss theory (Jeans 1925). According to this theory, a gravitational potential energy well is formed around a planet at the exobase level which traps the

[1] One should note that below the homopause level, the atmosphere is well mixed and each species adopts the same atmospheric scale height which is given by the average mass of an atmospheric particle, while above the homopause, due to molecular diffusion each atom or molecule follows its own scale height based on its mass.

planetary atmospheric constituents whenever the exobase temperature is much lower than the critical temperature for blow off ($T_c \sim 5000$ K for H and 10,000 K for H_2 on Earth). And only particles in the high energy tail of the Maxwellian distribution function of the atmospheric gas, having kinetic energies above the escape energy at the exobase, can overcome this energy barrier ("evaporate") and leave the gravitational field of the planet (e.g., Jeans 1925; Chamberlain 1963; Öpik 1963; Gross 1972).

3.2 Present and Early Venus

On Venus neutral density measurements were carried out during 1978–1980 at the solar maximum conditions ($F_{10.7} \sim 180$–200) and again in the fall of 1992 at the solar medium conditions during the pre-entry phase of NASA's Pioneer Venus Orbiter (PVO). Von Zahn et al. (1980) derived from the He number densities measured by the PVO Bus Neutral Mass Spectrometer (BNMS) a constant neutral gas temperature on Venus' dayside between 160–500 km of about 275–290 K by taking into account the altitude variation of the gravitational acceleration. Similar exospheric temperatures of about 290–300 K were inferred from the Orbiter Neutral Mass Spectrometer (ONMS) instrument (Nieman et al. 1979a, 1979b, 1980; Hedin et al. 1983; Fox and Sung 2001).

Moderate solar activity yields on Venus an average dayside exospheric temperature of ∼270 K. In situ measurements in the Venus upper atmosphere during the solar minimum derived from Magellan aerobraking data yield average dayside exospheric temperatures of ∼240–250 K (Keating et al. 1998).

Figure 5 shows our modelled temperature profiles in the 96% CO_2 Venusian thermosphere as a function of altitude for different solar XUV flux values. One can see from Fig. 5 that our model simulations for present Venus (XUV = 1) yield the exospheric temperature for medium solar activity conditions of ∼270 K which is in good agreement with the global empirical model of the Venus thermosphere based on the PVO neutral mass spectrometer measurements of Hedin et al. (1983) and the neutral gas mass spectrometer of the PVO multiprobe bus (Von Zahn et al. 1980; Nieman et al. 1979a, 1979b), as well as with model simulations by Bougher et al. (1999). The average exospheric temperature rises from about 270 K at present time (1 XUV) up to ∼600 K 3.8 Gyr ago (10 XUV), ∼2300 K 4.33 Gyr ago (50 XUV), and ∼8200 K 4.5 Gyr ago (100 XUV). Due to the higher thermospheric temperature the thermosphere expands and the exobase level moves upward from about 200 km (present time) to about 2200 km 4.5 Gyr ago. Figure 6 shows the calculated exobase temperature on Venus for a 96%, 72%, 48% and 10% CO_2 and N_2 atmosphere and various XUV flux values as a function of time.

If the exobase temperatures are higher than ∼4000 K, blow-off of atomic hydrogen occurs which results in diffusion-limited hydrodynamic outflow even for a 96% CO_2 atmosphere during ∼130 Myr after the Sun arrived at the ZAMS.

For lower CO_2 mixing ratios the thermospheric temperatures could be above the critical temperature at the exobase for atomic hydrogen of ∼4000 K for much longer time and extremely high exobase temperatures in excess of 10000 K ∼4 Gyr ago (15 XUV) could develop.

Chassefière (1996b), by applying a hybrid hydrodynamic-kinetic model for a pure atomic hydrogen atmosphere of a Venus-like planet, found self-consistent steady state solutions with a high Jeans loss at the exobase, elevated up to one planetary radius altitude (or more). His model incorporates hydrodynamic approach below the exobase and Jeans escape at the exobase. Apart from the solar XUV energy heating, it includes heating by the solar wind (energetic neutrals, ENs) which takes place near the exobase and supplies about 2/3 of the

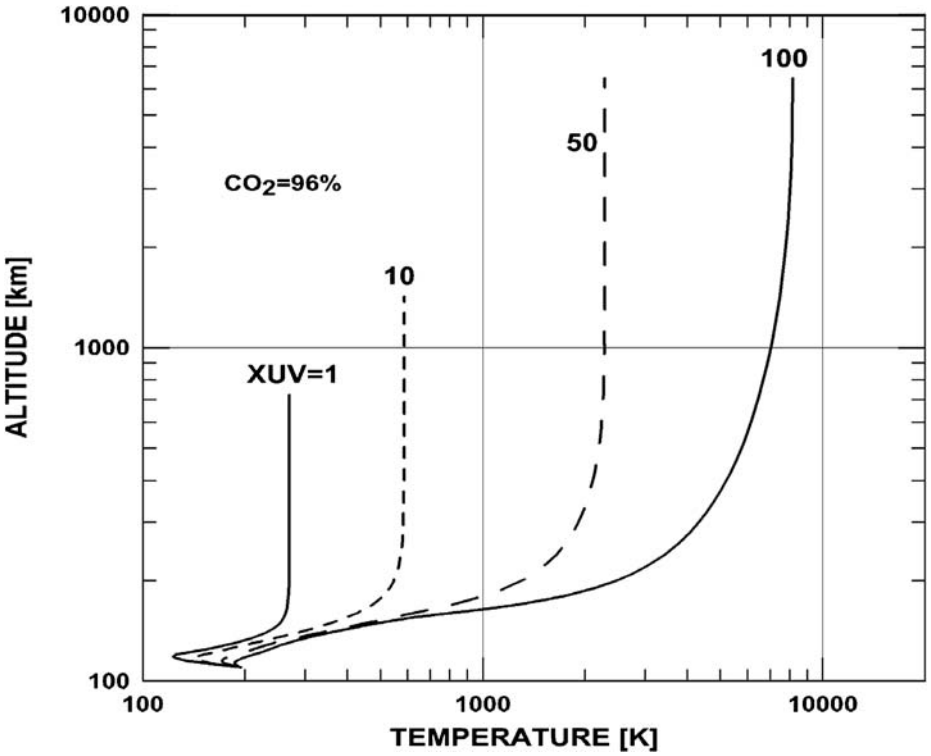

Fig. 5 Modelled temperature profiles in a 96% CO_2 thermosphere of Venus as a function of altitude for 1 XUV (present time), 10 XUV (∼3.8 Gyr ago), 50 XUV (∼4.33 Gyr ago), and 100 XUV (∼4.5 Gyr ago) flux values

escape energy. The model also includes a thermal energy input by the hydrogen upward flux through the lower boundary. The cooling mechanisms considered in the model are adiabatic cooling due to hydrogen escape flow and downward thermal conduction loss through the lower boundary at $z_0 = 200$ km. This model does not include IR-radiation cooling which can be present in a hydrogen-rich thermosphere due to H_3^+ ion (Yelle 2004) and also in the lower thermosphere due to CO_2. In the nominal case of the model with a moderate temperature T_{exo} at the exobase of about 750 K, Chassefière (1996b) found that intense hydrodynamic upward flow of hydrogen exists below the exobase for the present solar XUV conditions relayed by high Jeans escape flux at the exobase of 2×10^{11} cm^{-2} s^{-1}. This exobase temperature is not much higher, however, than $T_{exo} \approx 500$ K obtained from our Venus thermosphere model for present time solar condition and a low CO_2 level of 10%, as it is shown in Fig. 6. Also, it is not surprising that there is no hydrogen bulk outflow from our model thermosphere, since the atmosphere is assumed to be "dry", as explained before. However, the results of Chassefière (1996b) clearly indicate that an intense Jeans escape can provide an important contribution to the energy budget of a hydrogen-rich early Venus upper atmosphere and, thus, be an important factor for finding self-consistent hydrogen outflow solutions even for a present time solar XUV flux.

The present solar flux at Venus' orbit is about 1.91 times the solar constant of today, S_{Sun} ($S_{Sun} = 1360$ W m^{-2}), while the radiation flux according to the solar standard model on Venus orbit 4.5 Gyr ago was about 1.34 S_{Sun} (e.g., Gough 1977; Kasting et al. 1984;

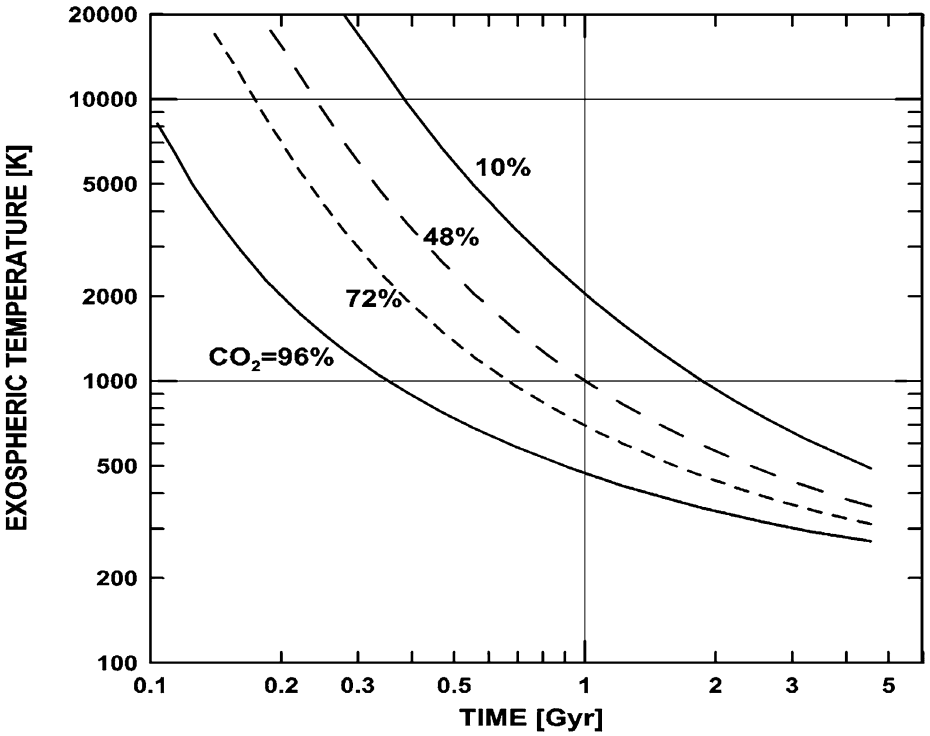

Fig. 6 Modelled venusian exobase temperatures for a 96% CO_2, for a 72% CO_2, for a 48% CO_2, and for a 10% CO_2 atmosphere as a function of the solar age and XUV flux

Lundin et al. 2007, this issue). Pollack (1971), Kasting et al. (1984) and Kasting (1988) studied runaway and moist greenhouse cases and their implications for the evolution of the atmospheres of early Earth and Venus.

Kasting (1988) found that the critical solar flux at which a runaway greenhouse effect occurs, or when a water ocean evaporates entirely, is about 1.4 S_{Sun} at Earth's orbit. This value is close to the expected solar flux incident on early Venus. Moreover, the climate models of Kasting (1988) indicate that the runaway greenhouse effect occurs under these conditions nearly independently of the amount of CO_2 in the atmosphere. For a CO_2 pressure, $P_{CO_2} \leq 10$ bar the critical solar flux value remains equal to 1.4 S_{Sun} and for a $P_{CO_2} \approx 100$ bar the S_{Sun} value increases only a slightly to 1.42 S_{Sun}.

The critical solar flux for which a runaway greenhouse effect could occur is found to be highly dependent on the presence of clouds (Kasting 1988). It was found that for clouds located at a pressure level of a few tens of a bar, the critical solar flux for a 50% and 100% cloud cover increases to about 2.2 S_{Sun} and ~4.8 S_{Sun}, respectively. From these results Kasting (1988) suggested that early Venus' surface was likely "cool" enough, so that a liquid water ocean could have been maintained before it evaporated.

Kasting and Pollack (1983) studied the hydrodynamic loss of water from a primitive H_2O-rich venusian atmosphere as a function of the H_2O mixing ratio at the mesopause level. They found that for H_2O mixing ratios of more than 7×10^{-4} atomic hydrogen becomes the major species at the exobase which moves then to greater distances, so that the exosphere becomes unstable to expansion, Jeans escape becomes inappropriate and hydrodynamic con-

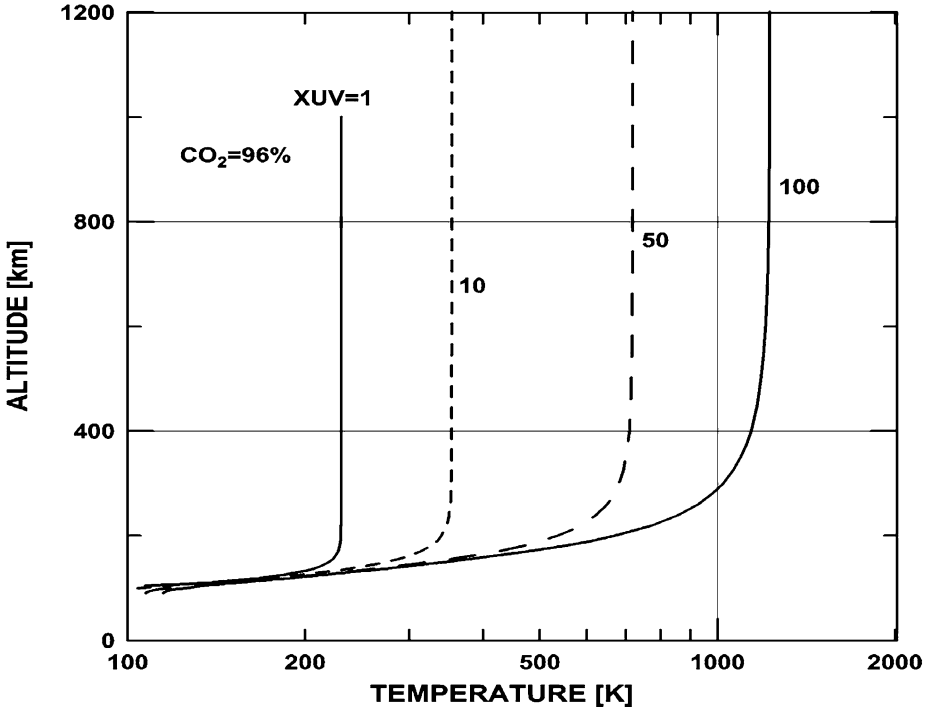

Fig. 7 Modelled martian temperature profiles in a 96% CO_2 thermosphere as a function of altitude for 1 XUV (present), 10 XUV (3.8 Gyr ago), 50 XUV (4.33 Gyr ago), and 100 XUV (4.5 Gyr ago) flux values for a low heating efficiency of ~8%

ditions have to be considered. They also found that on early Venus atomic hydrogen could escape for the H_2O mixing ratio of 0.0063 at 10 XUV with a flux of $\sim 3.5 \times 10^{11}$ cm^{-2} s^{-1}. Extrapolation of their results for the 100 XUV level yields a flux of $\sim 3.8 \times 10^{12}$ cm^{-2} s^{-1}. If the mixing ratio of H_2O were higher (0.055–0.46) because of the runaway greenhouse, hydrogen escape flux values of the order of ~ 1–3.5×10^{12} cm^{-2} s^{-1} could be reached for 8–16 times higher XUV fluxes (Kasting and Pollack 1983) and of ~ 1.3–2.7×10^{13} cm^{-2} s^{-1} for 100 XUV (Kulikov et al. 2006).

By using these H escape fluxes, it can be estimated that the full amount of a terrestrial ocean could have escaped over a time period of about 50 Myr if the H_2O mixing ratio was as high as 0.46 and the solar XUV flux was about 70–100 times the present solar value. However, if large amounts of water had evaporated on early Venus, the remaining oxygen would need to be incorporated in the crust as FeO (Lewis and Prinn 1984; Rosenqvist and Chassefière 1995), or would need to be lost to space due to intense erosion by the dense solar wind of the young Sun (Kulikov et al. 2006).

3.3 Present and Early Mars

Exospheric temperatures inferred from the mass spectrometer data during low solar activity by the NASA Viking Landers 1 and 2 yielded values of about 180 K and 150 K, respectively (e.g., Nier and McElroy 1977; Hanson et al. 1977; Fox and Dalgarno 1979; Barth et al. 1992; Fox and Sung 2001). A similar temperature value during low solar activity of 153

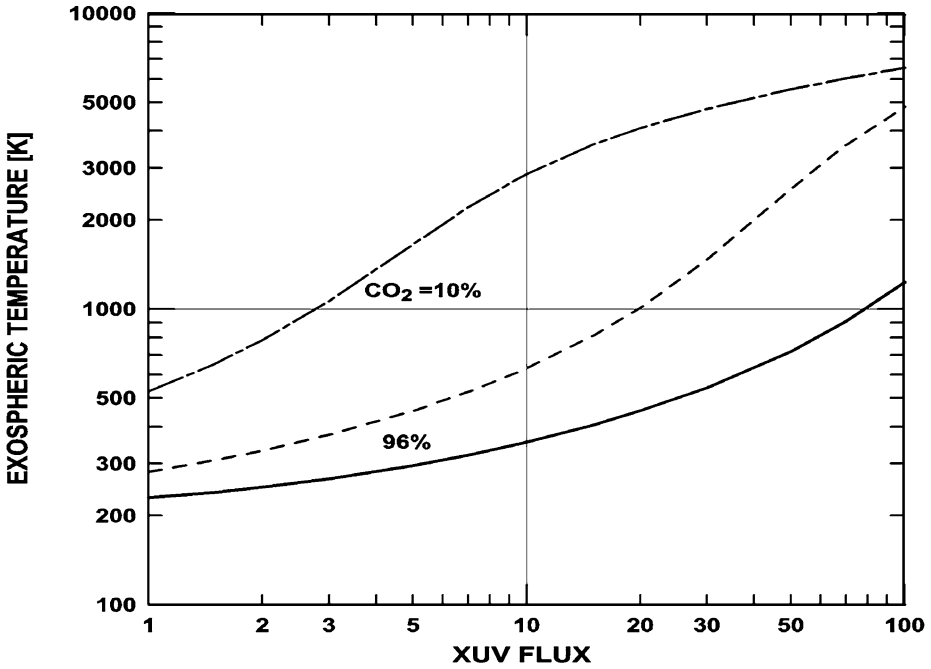

Fig. 8 Modelled martian exospheric temperatures as a function of solar XUV flux values for a 96% CO_2 atmosphere and for a heating efficiency of ∼8% (*solid line*) and ∼32% (*dashed line*). The *dashed-dotted line* corresponds to a martian atmosphere with a lower CO_2 mixing ratio of ∼10%. The *horizontal thin solid line* corresponds to the H blow-off temperature of ∼1000 K and the *vertical solid line* marks the conditions ∼3.8 Gyr ago

K was modelled by using thermospheric neutral gas data from the descent measurement of NASA's Mars Pathfinder in 1997 (Schofield et al. 1997; Magalhaes et al. 1999; Bougher et al. 2000). By reproducing aerobraking data of NASA's Mars Global Surveyor (MGS) with thermospheric models, one obtains exospheric temperatures of ∼220–230 K during moderate solar activity conditions (e.g., Keating et al. 1998; Bougher and Keating 1999) and ∼240 K for high solar activity.

Figure 7 shows our modelled temperature profiles in a 96% CO_2 martian thermosphere as a function of altitude for different XUV flux values. One can see from Fig. 7 that our model simulations for present Mars result in the exospheric temperature for medium solar activity conditions of ∼220 K which is in good agreement with the temperatures inferred from the aerobreaking data of MGS.

Figure 8 illustrates the exobase temperature on Mars for a 96%, and 10% CO_2 and N_2 atmosphere as a function of solar XUV flux for the lower and upper limits of the heating efficiency from ∼8% through ∼32% adopted in our simulations as discussed by Fox (1988). These derived estimates of the exobase temperature for early Mars show a large degree of uncertainty which results from our present poor knowledge of many essential parameters needed for modelling, including atmospheric composition and variation of minor species, heating efficiency, etc.

The blow-off temperature for atomic hydrogen on Mars is about ∼1000 K. Depending on an initial CO_2 mixing ratio and exobase altitude, atomic hydrogen could have been under diffusion-limited hydrodynamic blow-off conditions even for an extremely low heating effi-

ciency of about 8% and a 96% CO_2 atmosphere during about 100 Myr after the Sun arrived at the ZAMS. For the maximum heating efficiency of ∼32% the blow-off period could have lasted for ∼400 Myr. If an early martian atmosphere had a lower CO_2 abundance with a 10% mixing ratio, for example, shortly after its volatile outgassing, then the blow-off period could have lasted much longer and would have resulted in higher exobase temperatures and larger thermal loss rates of heavier species like H_2, He, C, N and O. However, due to greater orbital distance, as compared to Venus and Earth, which results in a lower solar luminosity of ∼0.25 S_{Sun} on early Mars, the hydrodynamic loss of atomic hydrogen during a blow-off period could have been less efficient for Mars than for both these planets.

4 Non-Thermal Atmospheric Loss Processes From Non- or Weakly Magnetized Planets

4.1 Photochemically Produced "Hot" Neutrals and Planetary Coronae

It is known from spacecraft observations and model simulations that photochemical reactions like dissociative recombination where a positive molecular ion recombines with an electron so that the neutral molecule dissociates, and photodissociation where a photon dissociates molecular neutrals, are important sources of suprathermal or energetic H, C, N, O, and CO in the exospheres of present Venus and Mars (e.g., McElroy et al. 1982; Nagy et al. 1981; Rodriguez et al. 1984; Ip 1988; Nagy et al. 1990; Lammer and Bauer 1991; Zhang et al. 1993a; Jakosky et al. 1994; Fox and Hać 1997; Luhmann et al. 1997; Fox and Hać 1997; Kim et al. 1998; Lammer et al. 2000b; Fox and Bakalian 2001; Lammer et al. 2003a, 2006).

The released "hot" or energetic atoms may reach eventually the same temperature as the background atmosphere through a series of elastic collisions with the main background gas such as CO_2 or O. The effective cross-section area for these inelastic collisions is, however, negligibly small at these low energies. After their release the atoms may collide with the neutral background gas, may change directions, loose their energy, or may travel long distances in the upper atmosphere without collisions. Finally, the newly generated "hot" atoms which reach the exobase with energies larger than the escape energy from the planet, are lost, while particles with lower energy are responsible for the formation of extended neutral exospheres, so-called planetary coronae, which interact with the solar wind plasma.

Figure 9 displays the sum of "hot" and "cold" O number density distributions which originate from dissociative recombination of O_2^+ molecular ions for 1 XUV (present), 10 XUV (3.8 Gyr ago), 50 XUV (4.33 Gyr ago) and 100 XUV (4.5 Gyr ago) flux values on Venus (Kulikov et al. 2006). The hot oxygen component is calculated from the modelled O_2^+ ion number density by means of the two-stream Monte Carlo model of Lammer et al. (2000b). For the calculation of the O_2^+ ion profiles as a function of the XUV flux the ionospheric model of Shinagawa et al. (1987) is applied to our calculated neutral density profiles (see also Kulikov et al. 2006), with the rate coefficients for chemical reactions updated by using the data of Fox and Sung (2001). Photoionization rates of neutral gases are calculated by using the solar radiation model, photoabsorption cross sections, and photoionization cross sections of Shunk and Nagy (2000). The photoionization rates for different XUV fluxes are calculated using the photoabsorption and photoionization cross sections and multiplying the present day solar XUV spectra. The photoelectron impact ionization rates of N_2 and O are taken from Richards and Torr (1988). Higher solar XUV radiation produces denser ionospheric layers and more dissociated "hot" atoms result in a denser corona. The densities

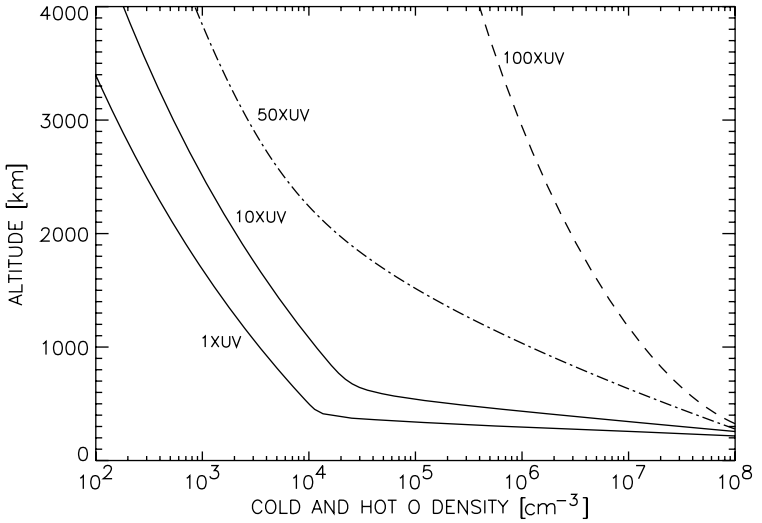

Fig. 9 Sum of "cold" and "hot" O number densities on Venus as a function of altitude for 1 XUV (present), 10 XUV (3.8 Gyr ago), 50 XUV (4.33 Gyr ago), and 100 XUV (4.5 Gyr ago) fluxes

of "cold" and "hot" oxygen populations above the exobase are obtained by extrapolations based on Chamberlain's equations (Chamberlain 1963). The density contribution of "hot" O atoms to the formation of planetary "hot" corona is mainly important for flux values $\leq$50 XUV, as can be seen from Fig. 9. The "flat" part of the profiles corresponds to the colder background atmosphere, while the "steep" part is due to the more energetic "hot" particles. For XUV fluxes >50, the temperature of the heated background gas approaches that of the hot particles and eventually the temperatures of both populations become indistinguishable.

4.2 Solar Wind Induced Ion Pick up

The main difference between present Venus and Mars compared to Earth is the lack of a significant intrinsic magnetic field, allowing the incident energetic solar wind particles to directly interact with their upper atmospheres. The solar wind plasma flow around planetary obstacles with no or weak intrinsic magnetic field have been studied extensively by using gas-dynamic convection magnetic field models (e.g., Spreiter and Stahara 1980), semi-analytical magnetohydrodynamic (MHD) flow models (e.g., Biernat et al. 2001), or hybrid models (e.g., Terada et al. 2002; Kallio and Janhunen 2003). The model results have been compared with observational data obtained from spacecraft, especially for Mars and Venus.

Neutral atoms and molecules above the ionopause can be transformed to ions via charge exchange with solar wind particles, XUV radiation and electron impact. These newly generated planetary ions are accelerated to higher altitudes and energies by the interplanetary electric field and incorporated or picked up by the solar-wind plasma flow past the planetary obstacle to space, where they are lost from the planet (e.g., Lundin et al. 1989, 1990, 1991, 2004; Lichtenegger and Dubinin 1998; Biernat et al. 2001; Lammer et al. 2003a; Terada et al. 2002; Kulikov et al. 2006; Lammer et al. 2006). These picked up ions can also collide with the background gas and may sputter atmospheric species to energies above the escape energy from the planet.

4.3 Atmospheric Sputtering

Sputtering refers to a mechanism by which incident energetic particles (mostly ions) interact with the upper atmosphere, resulting in ejection of atmospheric species. Sputtering has been recognized as an important source of atmospheric loss in the case of Mars and of less importance for larger planets like Venus (Luhmann and Kozyra 1991). In particular during the early phase of the Solar System, atmospheric sputtering is thought to be significant for loss of martian water and other atmospheric constituents (e.g., Luhmann et al. 1992; Kass and Yung 1995, 1996; Johnson and Liu 1996; Hutchins et al. 1997; Luhmann 1997; Johnson et al. 2000; Leblanc and Johnson 2001, 2002; Lammer et al. 2003a; Chassefière and Leblanc 2004).

4.4 Viscous Processes

Apart from non-thermal loss processes like ion pick up and atmospheric sputtering, ionospheric erosion due to plasma instabilities and momentum transfer (solar wind plasma forcing) are additional important loss processes from non-magnetized planetary bodies. Measurements by the PVO spacecraft (orbiting Venus) revealed a number of characteristic ionospheric structures that may be signatures of solar wind-ionosphere interaction processes (e.g., Brace et al. 1982; Russell et al. 1982). Among them are wavelike plasma irregularities observed at the top of the dayside ionosphere and plasma clouds observed above the ionopause, primarily near the terminator and further downstream. More detailed analysis of several detached plasma clouds has shown that the ions within the clouds themselves are ionosphere-like in electron temperature and density (Brace et al. 1982). When such plasma clouds are seen far above the ionosphere, they are clearly separated by an intervening region of ionosheath plasma. Note that the ionosheath is the region between the bow-shock and the ionopause. The latter is the transition region between tangential solar wind flow around the ionosphere and the ionosphere itself. The properties of the ionosheath are strongly affected by the presence of the neutral atoms extending above the ionopause.

This large separation in a direction perpendicular to the ionosheath flow suggests that the ionospheric plasma in the clouds must have originated in the ionosphere upstream on the dayside, indicating that plasma instabilities may occur at the venusian ionopause. In the region adjacent to the sunward side of the magnetopause, where the magnetic field significantly increases and simultaneously the plasma density decreases (the so-called magnetic barrier), plasma is accelerated by a strong magnetic tension directed perpendicular to the magnetic field lines. This magnetic tension forms specific types of plasma flow stream lines near the ionopause, which are orthogonal to the magnetic field lines. This process favors the appearance of the Kelvin–Helmholtz instability[2] that can detach ionospheric plasma from a planet in the form of detached ion clouds. In studies related to terrestrial planets one can treat the solar wind flow past the planetary obstacle using a magnetohydrodynamic model which was applied successfully for the case of the solar wind flow around Venus and Mars (Lammer et al. 2003b; Penz et al. 2004; Lammer et al. 2006).

[2]A Kelvin–Helmholtz instability can develop in case of a velocity difference across the interface between two fluids. At Venus, this instability may occur close to the ionopause due to the interaction between the solar wind and the ionosphere.

Table 1 Escape rates in units of [s^{-1}] of H, H_2, O and O^+ for moderate solar activity conditions at present Venus (see Lammer et al. 2006, and references therein). The asterisk in the notations H* and O* indicates "hot" neutral atoms produced in ionospheric photochemical reactions

Loss process / species	Loss rate
Jeans: H	2.5×10^{19}
Photochemical reactions: H*	3.8×10^{25}
Photochemical reactions: O*	negligible
Electric field force: H^+	$\leq 7 \times 10^{25}$
Ion pick up: H^+	1×10^{25}
Ion pick up: H_2^+	$<10^{23}$
Pick up: O^+	1.6×10^{25}
Detached plasma clouds: O^+	$5 \times 10^{24} - 1 \times 10^{25}$
Sputtering: O	6×10^{24}

4.5 Atmospheric Loss over Venus' History

4.5.1 Atmospheric Escape from Present Venus

Atmospheric escape from the upper atmosphere of Venus is mainly influenced by the loss of hydrogen and oxygen caused by the interaction of the solar XUV radiation and particle flux with the unprotected upper atmosphere. Lammer et al. (2006) estimated the total hydrogen and oxygen loss rates from present Venus shown in Table 1 and found that the ion pick up and ionospheric erosion caused by the Kelvin–Helmholtz plasma instability which is of the order of 10^{25} s^{-1} may be the most efficient escape processes for O^+ ions on Venus. Thermal atmospheric escape processes and atmospheric loss by photochemically produced O atoms yield negligible loss rates. On the other hand, photochemical production of hot H atoms is a very efficient loss mechanism for hydrogen on Venus with a global average total loss rate of about 3.8×10^{25} s^{-1}. This estimate is in agreement with a Donahue and Hartle (1992) result and of the same order, but less than estimated by Hartle and Grebowsky (1993) for an H^+ ion outflow from the Venus' nightside of about 7.0×10^{25} s^{-1} due to acceleration by an outward electric polarization force related to ionospheric holes.

Their study indicates that on Venus, due to its larger mass and size compared to Mars, the most important atmospheric escape processes of oxygen involve ions, and they are due to the interaction with the solar wind. The obtained results indicate that the ratio of H/O escape to space from the venusian upper atmosphere is about 4, and is in a much better agreement with the stoichiometrical H/O escape ratio of 2 : 1, which is not the case on Mars (Lammer et al. 2003a). However, we expect that a detailed analysis of the outflow of ions from the Venus' upper atmosphere as is expected to be measured by the Automatic Space Plasma Experiment with a Rotating Analyzer-4 (ASPERA-4) and the Venus Express magnetometer (VEX-MAG) instruments aboard ESA's Venus Express will lead to more accurate atmospheric loss estimations and better understanding of the planetary water inventory.

4.5.2 Solar Wind Induced Atmosphere Erosion and Water Loss over Venus' History

Present Venus is an extremely dry planet containing very little H_2O vapor (about 200–300 ppm Hoffman et al. 1980; Moroz et al. 1979; Johnson and Fegley 2000) in its atmosphere. The analysis of the Pioneer Venus Large-probe Neutral Mass Spectrometer (LNMS) data indicated that Venus' atmosphere is enriched in D over H relative to Earth by a factor of $\sim 120 \pm 40$, implying that Venus was once more "wet". McElroy et al. (1982) used the present hydrogen escape rates and showed that these loss rates over 4.5 Gyr would imply

a lower limit of water on Venus of ∼0.3% of a terrestrial ocean (TO). However, Donahue and Hartle (1992) and Hartle et al. (1996) deduced the amount of water lost from Venus from the measured D/H ratio based on ion mass spectrometer measurements in a range of an equivalent TO-depth of several meters to tens of meters.

For the prediction of the amount of primordial water on early Venus one has to consider two possibilities. The first hypothesis assumes that early Venus was formed from condensates in the solar nebula that contained little water (e.g., Holland 1963; Lewis 1970, 1972, 1973, 1974; Lewis and Prinn 1984), while the second hypothesis argues, in agreement with previous theories (e.g., Dayhoff et al. 1967; Walker 1975), for a water abundance more comparable to that on Earth and Mars (e.g., Wetherill 1981; Donahue and Pollack 1983; Kasting and Pollack 1983; Morbidelli et al. 2000; Raymond et al. 2004).

The supply of water to the venusian atmosphere by comets was studied by Lewis (1974), Grinspoon and Lewis (1988) and more recently by Chyba et al. (1990). Grinspoon and Lewis (1988) argued that the present water content of Venus may be in a steady state where the loss of hydrogen to space is balanced by a continuous input of water from comets or from delayed juvenile outgassing. It is important to note that in the case of an external water delivery no increase of Venus' past water inventory is required to explain the present day observed D/H isotope fractionation. The enrichment of D could conceivably have started out of more or less "dry" conditions, as originally was suggested by Lewis (1972).

However, the initial water inventory on early Venus may have been larger, because a substantial amount of water is required to explain the onset of the large greenhouse effect observed at present (e.g., Shimazu and Urabe 1968; Rasool and Bergh 1970; Donahue et al. 1982; Kasting and Pollack 1983; Chassefière 1996a; Chassefière 1996b). From these considerations one may expect that the early outgassing of water from Venus should have been much more efficient than it is at present to generate an equivalent amount of a TO (e.g., Hunten et al. 1987).

Kulikov et al. (2006) investigated for the first time the O^+ ion pick up loss rates over Venus' history and found that a dense solar wind of the young Sun could easily remove the expected amount of oxygen which could have been left from an XUV-driven hydrodynamically escaping ocean (see Table 2). Chassefière (1996a) showed that if Venus' H_2O-rich atmosphere hydrodynamically evaporated during the first 100 Myr, about 120 bar of H_2O and ∼36 bar of oxygen could be lost to space along with the planetary hydrogen wind.

However, Chassefière (1996a) expected that about 85 bar of oxygen should have remained in the atmosphere and could have oxidized the surface minerals from FeO to Fe_2O_3 to a depth from a few kilometers to tens of kilometers, depending on the original water amount. On the other hand, Venus' present surface is relatively young (∼500 Myr), which implies periodic efficient volcanic reforming processes. The capability to oxidize the surface by these processes is yet unknown and should be studied in the future.

As seen from Table 2, a solar wind with plasma densities exceeding that of the moderate solar wind case of Wood et al. (2002) could have removed such amounts of oxygen before 4.5 Gyr even if we neglect the pick up loss process during the expected hydrogen blow-off period in the first 100 Myr. However, the loss rate estimates by Kulikov et al. (2006) may represent a lower limit, because only the ion pick up process was studied. It can be expected that atmospheric sputtering by a dense solar wind and erosion of ionized atmospheric species by plasma instabilities might increase the total loss rate from the early Venus' atmosphere.

If one assumes that Venus was "dry" over its past, our results have several implications. If the solar wind of the young Sun was emitted within the ecliptic plane, the unmagnetized early Venus could have lost up to 200–300 bar of oxygen due to ion pick up by expected moderate to high solar wind plasma fluxes. Because present Venus has its expected original

Table 2 Pick up O^+ ion loss in units of [bar] by the solar wind integrated backwards over time for the period from 3.6 to 4.6 Gyr ago

t [Gyr] ago	3.6	3.8	4	4.2	4.4	4.5	4.6
Maximum solar wind	0.067	0.13	0.3	1.1	14	117	276
Moderate solar wind	0.036	0.066	0.17	0.43	3.5	25	59
Minimum solar wind	0.016	0.028	0.062	0.16	1	6.4	14.5

Note that the solar wind plasma interaction boundary with the extended early Venus atmosphere is assumed to be one atomic oxygen scale height below the exobase level. The shown cases are for the maximum, moderate and minimum solar wind densities of Wood et al. (2002) and Lundin et al. (2007, this issue)

CO_2 inventory of about 100 bar in the atmosphere, it is unlikely that the initial CO_2 reservoir was about 200–300 bar higher.

For overcoming this problem one can postulate that the early venusian atmosphere may have been protected during the active period of the young Sun by a strong Earth-like magnetic field, or that the early solar wind was emitted off the ecliptic plane during the first 300–500 Myr after the Sun arrived at the ZAMS (Wood et al. 2005). For the history of a possible intrinsic magnetic field on early Venus, we rely completely on theories of planetary magnetism. Stevenson et al. (1983) calculated the thermal evolution of the core by assuming that the energy available for a dynamo generation is equal to the ohmic dissipation and found that it may have been possible that the geophysical conditions on early Venus generated a magnetic moment 4.5–4.6 Gyr ago of about 0.8–1.4 $\mathcal{M}_e$, where $\mathcal{M}_e$ is the present magnetic moment of the Earth. The obtained magnetic moments decreased very fast to values of about $\leq$0.4 $\mathcal{M}_e$ after 200 Myr. Another alternative would be that Venus outgassed its main atmosphere after the first 200 Myr which would be much later than expected for early Earth.

4.6 Atmospheric Loss over the Mars' History

4.6.1 Atmospheric and Water Loss During the Past 3.5 Gyr

The present thin martian atmosphere with an average surface pressure of $\sim$7 mbar has been one of the great puzzles in our Solar System. Ancient fluvial networks on the surface of Mars suggest that it might have been warmer and more wet billions of years ago, implying a much higher atmospheric surface pressure (e.g., Kasting 1991; Forget and Pierrehumbert 1997). Surface features resembling massive outflow channels provide evidence that the martian crust contained the equivalent of a planet-wide reservoir of H_2O up to 150–200 meters deep (see, e.g., Carr 1987; Head III et al. 1999).

Since Mars did not have an appreciable intrinsic magnetic field during the past 4 Gyr (e.g., Acuña et al. 1998, 1999; Connerney et al. 1999), its atmosphere could be eroded due to the solar radiation and plasma impact.

Table 3 summarizes the modelled non-thermal atmospheric loss rates of heavy atmospheric species (O, C, CO, CO_2, O^+) from Mars over the past 3.5 Gyr. Assuming a fully active self-regulating coupling mechanism between O and H and integrating the water loss rates from Mars during the past 3.5 Gyr one obtains an amount of water equivalent to a global H_2O ocean with a depth of $\leq$12–15 m 3.5 Gyr ago (Lammer et al. 2003a, 2003b). Note that this H_2O amount could have been present also as ice if the climate conditions during the past 3.5 Gyr did not allow water to be liquid on the surface (Squyres and Kasting 1994;

Table 3 Escape rates in [s^{-1}] of O, O^+, CO_2 and CO are shown for present (1 XUV), 2.7 Gyr ago (3 XUV) and 3.5 Gyr ago (6 XUV) epochs for moderate levels of solar activity (Lammer et al. 2003a). The sputter loss rates for O, CO_2 and CO are calculated from the sputter yields of Table 1 of Leblanc and Johnson (2002) and incident particle pick up fluxes from Lammer et al. (2003a). The O loss rates produced by dissociative recombination for 1 XUV are based on the results of Kim et al. (1998), while the 3 XUV and 6 XUV loss rate values of hot O atoms are from Luhmann (1997). The present C loss rates which originate from dissociative recombination are taken from Fox and Bakalian (2001) and are extrapolated for the 3 and 6 XUV cases. O^+ ion loss rates estimated for momentum transport and detached ionospheric plasma clouds are taken from Lammer et al. (2003b) and Penz et al. (2004)

Loss process / species	Present	2.7 Gyr ago	3.5 Gyr ago
Pick up: O^+	3.0×10^{24}	4.0×10^{25}	8.3×10^{26}
Dissociative recombination: O	6.0×10^{24}	3.0×10^{25}	8.0×10^{25}
Dissociative recombination: C	8.0×10^{23}	4.2×10^{24}	1.3×10^{25}
Sputtering: O	3.5×10^{23}	1.3×10^{25}	1.5×10^{27}
Sputtering: CO_2	5.0×10^{22}	2.3×10^{24}	4.0×10^{25}
Sputtering: CO	3.7×10^{22}	2.0×10^{24}	2.5×10^{25}
Momentum transport: O^+	$\leq 10^{25}$	$\leq 2 \times 10^{26}$	$\leq 3 \times 10^{27}$
Plasma clouds: O^+	$\sim 10^{24}$	$\sim 8 \times 10^{24}$	$\sim 3 \times 10^{27}$

Wänke and Dreibus 1994). However, all atmospheric escape processes where ions are involved (ion pick up, atmospheric sputtering, momentum transport, plasma clouds) should have been reduced significantly due to the protection by the putative early martian magnetic field (Hutchins et al. 1997).

4.6.2 Magnetic Field Protection of the Early Martian Atmosphere

Planetary magnetic dynamo theory predicts that the strength of a magnetic moment depends on the planetary rotation rate, the core radius and input energy (either thermal, chemical or gravitational) to drive vigorous internal convection inside the core (e.g., Busse 1976; Stevenson et al. 1983; Schubert and Spohn 1990; Dehant et al. 2007, this issue).

The available data obtained by MGS on an early martian magnetic field are mainly restricted to measurements related to the presence of significant local, small-scale, crustal remnant magnetization (Acuña et al. 1998, 1999; Connerney et al. 1999). Investigations of martian meteoroids (Weiss et al. 2002) and observations and studies related to early martian plate tectonics and crustal evolution (Sleep 1994; Breuer and Spohn 2003) also support the idea of an early intrinsic martian magnetic field. The local magnetization appears mainly in the ancient southern highlands and is absent in the regions where large impacts occurred (like Hellas and Argyre). Since these impact basins were formed about 4 Gyr ago, it is generally argued that the martian dynamo ceased before this time (e.g., Acuña et al. 1999; Breuer and Spohn 2003).

Furthermore, magnetic studies of the martian SNC meteorite ALH 84001 revealed that about 4 Gyr old carbonates contained magnetite and pyrrhotite, which carried a stable natural remnant magnetization (Weiss et al. 2002). This result implies that Mars may have established a magnetic dynamo within 450–650 Myr after its formation with an intensity of an order of that on the present Earth. Moreover, these results support the theory that an ancient strong dynamo ceased about 4 Gyr ago. Simple model simulations based on ohmic dissipation suggest that the early martian magnetic moment could have been between the

maximum and minimum expected magnetic moment of ∼0.1–10 $\mathcal{M}_e$ (Stevenson et al. 1983; Schubert and Spohn 1990).

Hutchins et al. (1997) studied the effect of a paleomagnetic field, which was assumed to be cut off between 2.5 and 3.6 Gyr ago, on sputtering loss of martian Ar and Ne, as well as CO_2, from the present epoch (1 XUV) to 3.6 Gyr (6 XUV) ago. For the study of the magnetospheric compression due to the solar wind at earlier time periods they adopted the solar wind velocity model of Newkirk (1980) and the minimum expected magnetic moment of ∼0.1 $\mathcal{M}_e$ (Schubert and Spohn 1990). By applying the atmospheric model of Zhang et al. (1993a) and the sputter model of Luhmann et al. (1992), they found that even such a relatively weak magnetic moment, resulting in a small magnetosphere, could significantly decrease the ion production rate in the solar wind interaction region and, hence, the sputter loss.

However, it should be noted that Hutchins et al. (1997) considered only faster solar wind but they did not increase its number density to higher values as expected from the recent stellar observations by Wood et al. (2002, 2005). And a higher solar wind mass flux during the early time periods after the Sun arrived at the ZAMS could have moved the magnetopause closer to the planet, which may have resulted together with a more XUV heated and extended early martian atmosphere in higher non-thermal loss rates during the first Gyr.

To investigate the efficiency of the atmosphere protection by such an intrinsic magnetic moment as a function of the expected time-dependent stronger mass flux of the young Sun (Wood et al. 2002, 2005) in our modelled heated and extended early martian atmosphere, we calculated the subsolar magnetopause stand-off distance r_s by determining the magnetic and solar wind ram pressure balance condition at the subsolar point (e.g., Spreiter 1975; Slavin and Holzer (Slavin and Holzer 1979); Grießmeier et al. 2004, 2005)

$$r_s = \left[\frac{\mu_0^2 f_0^2 \mathcal{M}^2}{4\pi^2 (2\mu_0 n_{sw} m v_{sw}^2 + B_{IMF}^2)} \right]^{1/6}, \tag{12}$$

where $\mathcal{M}$ is the early martian magnetic moment, B_{IMF} is the interplanetary magnetic field (IMF), m is a proton mass, μ_0 and f_0 are magnetic permeability and magnetospheric form-factors, respectively. Note that the magnetic moment $\mathcal{M}$ and the IMF are assumed to be constant in our simulations, so that time variations of the stand-off distance may be only due to variations of the solar wind density n_{sw} and velocity v_{sw}.

Figure 10 shows the magnetopause stand-off distance r_s for the moderate expected solar wind density (Wood et al. 2002; Lammer et al. 2003a; Lundin et al. 2007, this issue) in the martian radii during the time period between 0.1–1 Gyr after the Sun arrived at the ZAMS for various values of magnetic moments in units of the present Earth's value ($\mathcal{M}_e$). The value of the solar wind velocity v_{sw} for the young Sun is taken from Newkirk (1980). One should note that the minimum solar wind plasma densities inferred from observations by Wood et al. (2002) will move the magnetic barrier further away from the planet, resulting in better atmospheric protection. If early Mars had a magnetic moment similar to that of present Earth, r_s 4.5 Gyr ago would have been ∼2.8 martian radii above the surface. An initial magnetic moment of ∼10 $\mathcal{M}_e$ (Schubert and Spohn 1990) results in r_s of ∼7 martian radii above the planetary surface. The lowest expected magnetic moment on Mars 4.5 Gyr ago of ∼0.1 $\mathcal{M}_e$ (Schubert and Spohn 1990) yields a magnetopause stand-off distance of ∼0.75 martian radii above the surface.

Only a very low magnetic moment of ∼0.01 $\mathcal{M}_e$ would result in a direct solar wind-atmosphere interaction like at present Mars during the first 200 Myr after the Sun arrived at the ZAMS. Due to the decreasing solar wind plasma density and velocity, r_s moves to

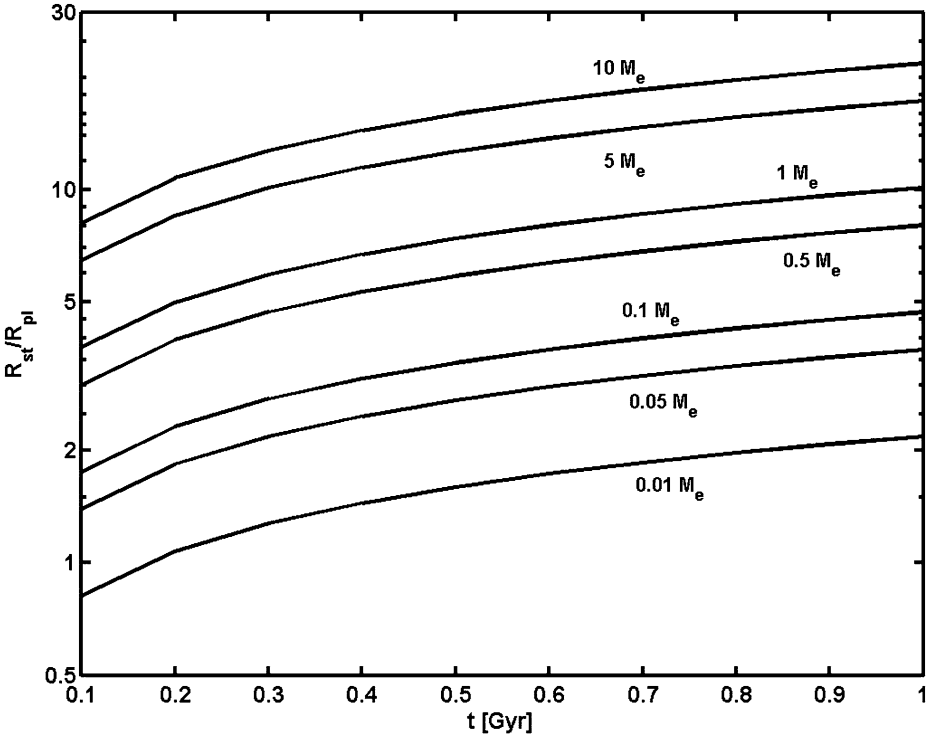

Fig. 10 Martian subsolar magnetopause stand-off distance for moderate solar wind density (Wood et al. 2002; Lammer et al. 2003a; Lundin et al. 2007, this issue) in units of the martian radii over a time period of 0.1–1 Gyr after the Sun arrived at the ZAMS for various values of expected martian magnetic moments

further distances above the martian surface, resulting in r_s for 0.01 $\mathcal{M}_e$ of ∼1.2 martian radii 4 Gyr ago.

Figure 11 shows the magnetopause stand-off distance r_s related to an assumed weak magnetic moment which decreases from 0.1 $\mathcal{M}_e$ to 0.01 $\mathcal{M}_e$ during the first Gyr after the Sun arrived at the ZAMS for the maximum (dotted-line), moderate (solid-line) and minimum (dashed-line) expected solar wind plasma density of Wood et al. (2002) and Lundin et al. (2007, this issue). One can see that the maximum expected solar wind mass flux 4.5 Gyr ago would move the magnetopause stand-off location to a distance of ∼1.4 R_{st}/R_{pl} in units of the martian radii, and to ∼1.85 R_{st}/R_{pl} and ∼2.45 R_{st}/R_{pl} for the moderate and minimum expected mass flux. One can see that r_s during the first 0.5 Gyr due to the decreasing solar wind plasma density moves to much higher altitudes above the planetary surface. Under the above assumptions, ∼3.5 Gyr ago due to the decreasing magnetic moment, r_s moves to altitudes which are comparable to those during the first 200 Myr after the Sun arrived at the ZAMS.

For studying the atmospheric protection effect of the early martian magnetic field on O^+ ion pick up loss we use a numerical test particle model that includes particle motion in the environmental electric and magnetic fields based on the Spreiter-Stahara gas-dynamic model (Spreiter and Stahara 1980).

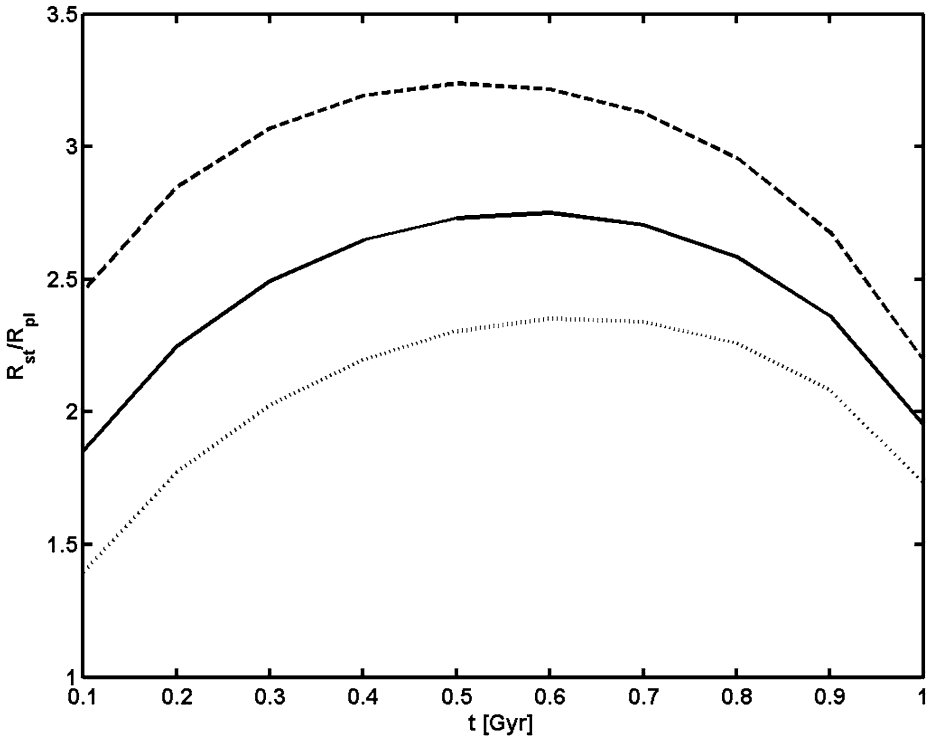

Fig. 11 Subsolar magnetopause stand-off distance for an early weak martian magnetic moment which decreases from 0.1 $\mathcal{M}_e$ to 0.01 $\mathcal{M}_e$ over the first Gyr. Maximum (*dotted-line*), moderate (*solid-line*) and minimum (*dashed-line*) expected solar wind plasma densities are taken from Wood et al. (2002), Lammer et al. (2003a), Lundin et al. (2007, this issue)

The production rates due to photoionization, electron impact and charge exchange are given by the following equations

$$Q_\gamma = \Phi_\gamma \sigma_\gamma n_O, \qquad Q_{ce} = \Phi_{sw} \sigma_{ce} n_O, \qquad Q_{ei} = \nu_e n_e n_O, \tag{13}$$

where Φ_γ and Φ_{sw} is the photon and solar wind flux, respectively, σ_γ and σ_{ce} is the ionization and charge exchange cross section of atomic oxygen, ν_e is the ionization frequency per incident electron, n_e the solar wind electron density and n_O the density of atmospheric oxygen. The energy dependent charge exchange cross sections are taken from Kallio et al. (1997) and the electron impact ionization frequencies from Cravens et al. (1987), where the electron temperature is approximated according to Zhang et al. (1993b). The total production rate Q of planetary O^+ is the sum

$$Q = Q_\gamma + Q_{ce} + Q_{ei} \tag{14}$$

and it is assumed that the ionized species are lost from the planet. This model reproduces successfully several ion distributions observed by the PVO on Venus (Luhmann 1993; Lammer et al. 2006) and the Soviet Phobos 2 spacecraft plasma measurements on Mars (Lundin et al. 1989, 1990, 1991; Lichtenegger and Dubinin 1998; Lichtenegger et al. 2002; Lammer et al. 2003a). For the calculation of the O^+ ion pick up fluxes 4.5 Gyr ago (100

XUV), 4.33 Gyr ago (50 XUV), and 3.8 Gyr ago (10 XUV) we use the modelled "cold" and "hot" neutral O densities shown in Fig. 12, which are obtained in a similar way as in Fig. 9.

One can see from Table 4 that the O^+ ion pick up loss rates 4.33 Gyr ago (50 XUV) are of the same order of magnitude and are most likely even lower than those about 3.5 Gyr ago due to the magnetic protection of the extended upper atmosphere. For the 100 XUV case 4.5 Gyr ago the moderate solar wind mass flux obtained by Wood et al. (2002) would yield O^+ ion pick up loss rates which are comparable with the expected O atom sputter loss rates 3.5 Gyr ago. The maximum expected solar wind mass flux would move the magnetic standoff distance to about 0.4 martian radii above the surface (4.5 Gyr b.p.). The corresponding O^+ ion pick up loss rate during this early period which is shown in Table 4, was about a factor of 10 larger than the O sputter loss rate ∼3.5 Gyr ago (see Table 3), resulting in oxygen loss

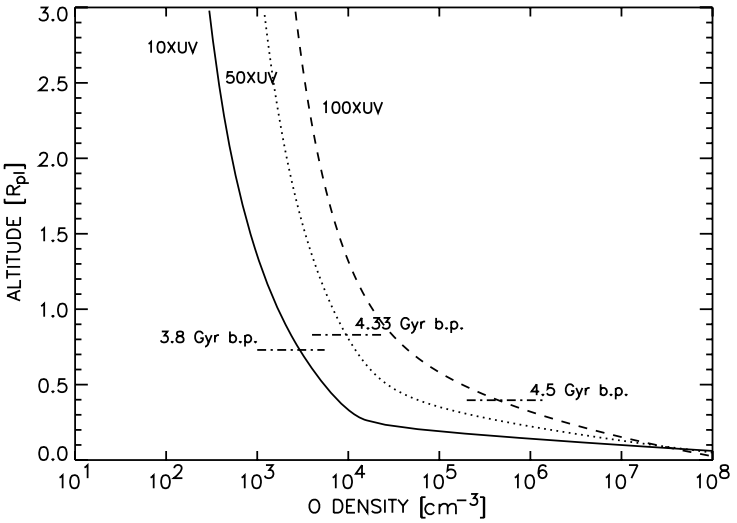

Fig. 12 Sum of "cold" and "hot" O number densities on Mars as a function of altitude in martian radii above the planetary surface for 10, 50, and 100 XUV fluxes (*solid, dotted* and *dashed lines*, respectively). The *dashed-dotted short lines* correspond to the magnetopause stand-off distances for the maximum expected solar wind mass flux (Wood et al. 2002; Lundin et al. 2007, this issue) and the expected minimum possible magnetic moment on early Mars of ∼0.1 $\mathcal{M}_e$ which is assumed to be decreasing to ∼0.01 $\mathcal{M}_e$ during the first Gyr after the Sun arrived at the ZAMS

Table 4 O^+ ion pick up escape rates in [s^{-1}] 4.5 Gyr ago (100 XUV) and 4.33 Gyr ago (50 XUV) and corresponding subsolar magnetopause stand-off distances r_s shown in Fig. 11 for maximum, moderate and minimum solar wind conditions (Wood et al. 2002; Lammer et al. 2003a; Lundin et al. 2007, this issue)

	4.5 Gyr ago [100 XUV]	4.33 Gyr ago [50 XUV]
$r_{s_{min}}$	$\approx 1.4 R_{pl}$	$\approx 2 R_{pl}$
Pick up: O^+	9.0×10^{26}	1.3×10^{26}
$r_{s_{mod}}$	$\approx 0.8 R_{pl}$	$\approx 1.4 R_{pl}$
Pick up: O^+	2.5×10^{27}	4.3×10^{26}
$r_{s_{max}}$	$\approx 0.4 R_{pl}$	$0.8 R_{pl}$
Pick up: O^+	1.5×10^{28}	1.5×10^{27}

over this time period of about 0.5 bar. Early martian magnetic moments more than 0.1 $\mathcal{M}_e$ or moderate solar wind plasma densities of the young Sun would yield negligible loss rates.

A test particle run for a 10 XUV case corresponding to a time period of ∼3.8 Gyr ago and a magnetic moment of the order of ∼0.01 $\mathcal{M}_e$ yields an O^+ ion pick up loss rate of the same order as that for an unprotected upper atmosphere at ∼3.5 Gyr ago (6 XUV). One should note that higher magnetic field strength of the IMF during the young Sun period (Newkirk 1980) would contribute to a higher compression of the magnetosphere. And a smaller magnetospheric stand-off distance given by (1) would result in an enhanced loss from the martian upper atmosphere.

Our model simulations for an unprotected martian upper atmosphere yield O^+ pick up loss rates, depending on the chosen solar wind mass flux values from ∼0.5 bar (minimum) up to ∼10 bar (maximum) during the first 200 Myr. However, one should note that an unprotected early martian upper atmosphere would also experience additional non-thermal loss processes like sputtering, plasma-instability-induced detached ionospheric clouds, and cool ion outflow due to the momentum transport effect (see Lundin et al. 2007, this issue). Therefore, in case of a late onset of the martian dynamo (Schubert et al. 2000) after the first 200 Myr combined with high exobase temperatures of more than 1000 K the planet could have lost up to several tens of bar.

Our results suggest that an early magnetic dynamo stronger than 0.1 $\mathcal{M}_e$ is necessary to protect the martian atmosphere during the first 200–300 Myr. Therefore, the results of our study are in general agreement with the Hutchins et al. (1997) results and indicate that an early magnetic dynamo could, probably, be strong enough to reduce the radiation and particle induced non-thermal atmospheric loss rates even for the XUV heated and expanded upper atmosphere by significant amounts.

4.6.3 Loss of CO_2 and Change in Surface Pressure

It is important to note that the total integrated mass loss of O atoms and ions shown in Table 3 may have not contributed to the total surface pressure change over the martian history, because the majority of escaping O and O^+ ions most likely had their origin from H_2O vapor but not from atmospheric CO_2 (see Lammer et al. 2003a and references therein; Amerstorfer et al. 2004). However, one should note that recent observations (Carlsson et al. 2006) and model simulations of atmospheric escape of carbon bearing species by various authors (Fox and Hać 1997; Leblanc and Johnson 2002; Lammer et al. 2003a and references therein; Chassefière and Leblanc 2004; Barabash et al. 2007) make it problematic that the surface pressure of the martian atmosphere could have reached values >0.3 bar at the end of the heavy bombardment, necessary for a greenhouse effect resulting in standing bodies of water on the martian surface.

Particle sputtering and photochemical reactions (dissociative recombination and photodissociation), however, could remove carbon bearing species (C, CO and CO_2), so that these processes would contribute to the loss of the martian atmosphere during the planets' past. Since ion pick up and sputtering depend on the solar wind mass flux, which was higher in the martian past (Lammer et al. 2003a; Lundin et al. 2007, this issue), sputtering could probably be more efficient during the early periods as long as no magnetospheric protection of the atmosphere was present.

By inspection of Table 3 it is seen that atmospheric loss due to dissociative recombination of ion species is more important for present Mars but was probably less important during earlier periods compared to sputtering and ion pick up, because the newly generated suprathermal neutrals have to move a longer distance in the XUV-heated and expanded

thermosphere before they can reach the exobase level. In such a case the "hot" particles experience more collisions which result in energy loss and lower escape rates. However, future studies should investigate in more detail the production of suprathermal neutrals by photodissociation, which could enhance the loss rates of "hot" atoms.

Impact erosion (e.g., Melosh and Vickery 1989; Brain and Jakosky 1998) and late impact accretion (e.g., Chyba et al. 1990) are additional processes that may have played an important role in the early martian atmosphere. Brain and Jakosky (1998) estimated the atmospheric loss due to impact erosion since the onset of the martian geologic record about 4 Gyr ago by using the size-frequency crater distribution N of craters having sizes more than 4 km ($N = 7 \times 10^{-4}$–3×10^{-3}) of Hartmann et al. (1981). They found an enhancement factor for the surface pressure ∼4 Gyr ago in the range of ∼2–9.

The result of Brain and Jakosky (1998) indicates that the total amount of atmosphere on Mars that was present at the onset of the geological record has been reduced by a factor of 2–9 due to large impact erosion, showing that early Mars may have lost from 50% to 90% of its original atmosphere due to impact erosion. Their result is different from the results of the previous studies by Melosh and Vickery (1989) who expected atmospheric loss rates due to impact erosion from early Mars in a range from 98% to 99.5%. However, for obtaining this result the crater density would need to be larger than ∼0.01 km^{-2}, which is almost one order of magnitude larger than the highest crater density values found on Mars.

It is important to note that Melosh and Vickery (1989) and Brain and Jakosky (1998) studied only the effect of impact loss and not impact delivery to the atmosphere. It may be possible that impact erosion and impact delivery are more or less in balance (private communications to H. Lammer by D. Brain and G. Neukum). If this is the case, then the major loss process should be the non-thermal escape related to a weak protecting early magnetic field or its late onset.

However, it may have been possible that Mars may have had a surface pressure at the end of the late heavy bombardment 3.8–4 Gyr ago of about ≤0.3–0.5 bar. The amount above the present 7 mbar surface pressure could have been lost due to sputtering and photochemical processes (e.g., Jakosky et al. 1994) and maybe due to ion pick up loss related to CO_2. Furthermore, CO_2 could be also lost due to weathering resulting in regolith deposits of the order ∼30–40 mbar (Zent and Quinn 1995) or of even higher levels of more than 100 mbar (Bandfield et al. 2003). Additionally, some tens of mbar could be sequestered as ice or clathrate in the polar areas (Mellon 1996). Such relatively small CO_2 surface-deposits would also be in agreement with the recent data obtained by ESA's Mars Express OMEGA-instrument that show that there may be no large amounts of carbonates on the martian surface (Biebring 2005). This result also indicates a strong early escape of most of the planets' CO_2 during the heavy bombardment period in agreement with our results.

5 Why Has the Earth Evolved Differently from Venus and Mars?

Figure 13 illustrates the results obtained from our comparative study of the influence of the XUV radiation and particle environment of the young Sun on the early upper atmospheres of Earth, Venus and Mars. From our study it seems likely that the early atmospheres (>4 Gyr ago) of the terrestrial planets contained high amounts of CO_2 (∼90–95%) that could substantially inhibit atmospheric loss, because CO_2 appears to be the most efficient IR-radiating molecule in planetary thermospheres. A high CO_2 mixing ratio could reduce high thermospheric temperatures, that would have a strong impact on thermal and non-thermal escape rates from the upper atmospheres. Therefore, we expect that the early atmosphere of

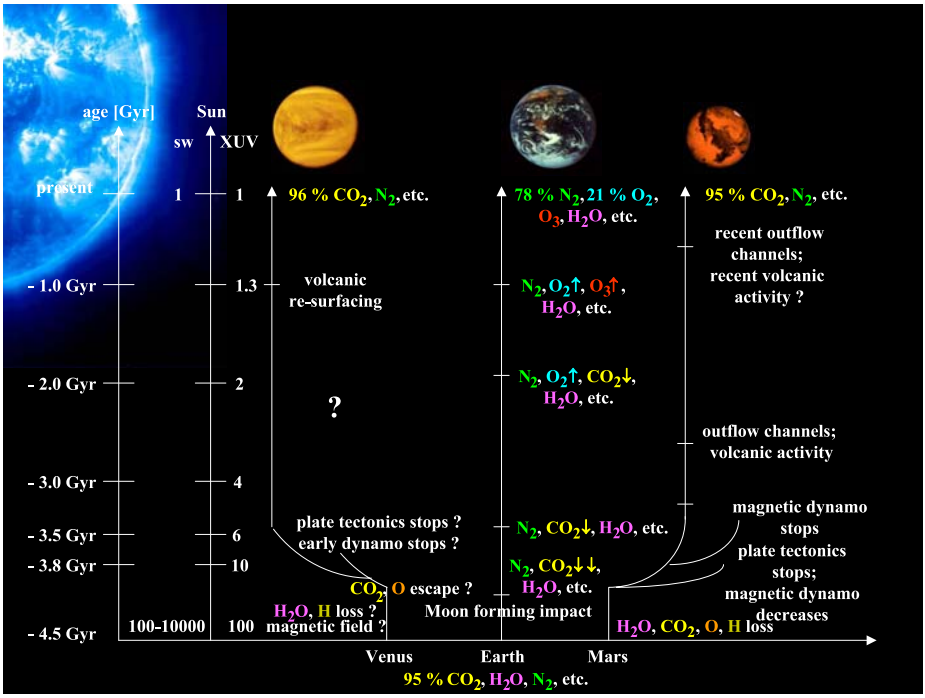

Fig. 13 Comparison of the expected evolutionary paths of the atmospheres and geophysical parameters of Venus, Earth and Mars under the influence of the solar particle and radiation environment

Earth ~4.5 Gyr ago could contain the present time Venus' and Mars' CO_2 mixing ratio of ~95%.

There are basically two scenarios conceivable for the generation of an early magnetic dynamo on Venus. The first possibility is that Venus had a superheated core with respect to the mantle due to the formation process. The cooling of such a superheated core would generate thermal convection in the core and consequently dynamo action. Such a thermal dynamo can be assumed to be active only during the first few hundred Myr. The second possibility could be that the young Venus experienced an early plate tectonic era which could have been driven by large H_2O inventories. Large original water inventories are essential for driving plate tectonics and keeping a magnetic moment active (Breuer and Spohn 2003). Active plate tectonics efficiently cools the mantle and core of terrestrial planets, so that an inner solid core and an outer liquid core can be formed and an early magnetic field can be easily generated. Unfortunately due to global volcanic reshaping of Venus' surface ~700–800 Myr ago it is difficult to find evidence that the planet once had active plate tectonics.

An unmagnetized early Venus may have lost a large amount of its atmosphere by non-thermal escape processes like ion pick up due to the dense solar wind plasma of the young Sun, or during an efficient blow-off phase for atomic hydrogen which originated probably from an evaporating H_2O ocean (Kulikov et al. 2006). In such a case the hydrodynamically escaping hydrogen wind would form a corona around early Venus similar to that discovered around evaporating short periodic hot exoplanets like HD209458 b (Vidal-Madjar et al. 2003). Dense solar wind of the young Sun would pick up mainly the evaporating atomic hydrogen, but heavier species like CO_2 at lower atmospheric levels would be protected and

stay mainly unaffected by non-thermal loss processes until the end of the hydrogen blow-off phase. Because the activity of the young Sun decreased very fast in time, Venus was able to keep the major part of its atmosphere until today. From these results we expect that an onset of a magnetic dynamo on early Earth was essential for protecting its hot and extended early upper atmosphere against erosion by the solar wind of the young Sun. In view of our present findings a late appearance of a strong magnetic dynamo on early Earth, suggested by Ozima et al. (2005) for the explanation of implanted terrestrial atomic nitrogen and noble gases in Lunar soils, seems rather unlikely. In such a case one might expect that without a protecting magnetic field, early Earth, like early Venus, could have lost up to a terrestrial ocean of water due to solar wind erosion, as O^+ ion pick-up loss calculations for early unmagnetized Venus by Kulikov et al. (2006) indicate. However, as drawing firm conclusions from our preliminary results is still not easy, a late onset of the terrestrial magnetic dynamo cannot be completely ruled out. But it would imply then that early Earth could have lost huge amounts of its water and atmosphere due to intense solar wind erosion.

There is observational evidence that early Mars ($\geq$4 Gyr ago) had a denser CO_2 atmosphere (e.g., McKay and Stocker 1989; Haberle et al. 1994; Brain and Jakosky 1998), a warmer climate (e.g., Forget and Pierrehumbert 1997; Haberle 1998; Manning et al. 2006), most likely liquid water running over its surface (e.g., Carr 1987; Head III et al. 1999; Baker 2001).

Depending on assumed solar wind parameters of the young Sun, the results of our study show that an early martian magnetic field could reduce the escape rate of atmospheric ions due to non-thermal loss processes very efficiently. On the other hand, our study indicates that Mars could have lost its whole atmosphere from several bar to several tens of bar due to a combined effect of the solar XUV heated upper atmosphere and a dense solar wind plasma flow of the young Sun if the planet were not protected by its magnetosphere during the first 200 Myr.

However, if one neglects the delivery of the atmosphere by impacts, one can expect that impact erosion may have been an efficient atmospheric loss process on early Mars during the heavy bombardment period (4–4.5 Gyr ago). This could have removed from about 50% to 90% of the early martian atmosphere (Brain and Jakosky 1998). On the other hand, if impact erosion was nearly in balance with impact atmospheric delivery, non-thermal loss processes combined with a weak early magnetic dynamo or a late onset of the dynamo (Schubert et al. 2000) (later than $\sim$200 Myr after the planet's origin) can explain the loss of the initial martian atmosphere. Future impact effect studies should, therefore, focus on the net delivery and loss of atmosphere during the heavy bombardment period. In addition, the atmospheric erosion and production rates due to asteroid and cometary impacts need to be combined with thermal and non-thermal loss calculations for early Mars models.

The remaining atmospheric species after the end of the heavy bombardment period may have been partly lost to space from the unprotected upper atmosphere due to non-thermal loss processes and the surface weathering into the ground, ice and clathrates (e.g., Mellon 1996; Zent and Quinn 1995; Bandfield et al. 2003).

Interestingly, Jakosky et al. (1994) found that efficient sputtering till the end of the heavy bombardment period can explain the isotopic $^{36}Ar/^{38}Ar$ ratio observed in the present martian atmosphere without requiring an epoch of very intensive hydrodynamic blow-off. However, the fractionation of Xe isotopes still requires an efficient hydrodynamic blow-off period (Jakosky et al. 1994; Pepin 1994; Becker et al. 2003).

As one can see from our Figs. 7 and 8, the early martian thermosphere and exosphere were hot enough due to the high XUV radiation, so that atomic hydrogen could experience blow-off. Depending on assumed atmospheric mixing ratios, available IR-coolers, warmer

climate in the lower atmosphere, and heavy impactors which contributed to thermospheric heating, large amounts of H_2O-related hydrogen may have escaped. During an early efficient blow-off period even heavy elements like Xe isotopes could have been dragged away with the intense hydrogen wind (e.g., Zahnle et al. 1990; Chassefière 1996a, 1996b; Becker et al. 2003). These blow-off conditions and high loss rates of hydrogen which could drag along with it heavier species, might have been much more important during the martian accretion phase (Dreibus and Wänke 1987).

It should be noted that our present understanding of loss processes which are induced by photodissociation, dissociative recombination, and atmospheric sputtering is based on estimates, since the loss rates are still not measured by spacecraft. Thus, the obtained loss rates are model dependent and have to be compared with future observational data and measurements by a Mars aeronomy orbiter. Also, Mars remains an attractive target for future space missions planned by NASA, ESA, Russia, etc., but so far no successful mission, which was dedicated to a study of the martian thermosphere-exosphere environment was launched. Such a mission should study in detail temperature, isotopes, cold and hot particle populations, escape fluxes of photochemically produced "hot" neutrals, ions, including isotopes, also ionopause loss processes and how they depend on the solar XUV activity. However, the missing data which may help us to understand the evolution of the early martian magnetic dynamo, its surface pressure, atmospheric sputtering and photochemical loss processes, etc. over the planets' history can only be procured by using a comprehensive package of instruments such as the one proposed for a Mars Magnetic and Environmental Orbiter (MEMO).

By comparing Venus and Mars with early Earth (Fig. 13), we find that expected high CO_2 abundance on early Earth might have been substantially reduced due to weathering from the atmosphere onto the surface and seafloor mainly during the first 500 Myr. Fortunately, the high XUV radiation of the young Sun decreased from ∼100 times higher value 4.5 Gyr ago (see Ribas et al. 2005; Lundin et al. 2007, this issue) to a ∼10 times higher value 3.8 Gyr ago and about 6 times higher value 3.5 Gyr ago than that of today.

At these lower XUV radiation fluxes 3.5–3.8 Gyr ago much lower CO_2 mixing ratios (∼1%) were able to substantially cool the upper atmosphere of Earth and to keep the exobase temperature below the critical level for hydrogen blow-off, so that the atmosphere and planetary water inventory could not be completely lost. Interestingly, these time periods correlate with the expected origin of the first life-forms which supposedly changed the Earth atmospheric composition to its present state.

6 Conclusion

We presented a comparative study of the influence of the solar radiation and particle environment of the young Sun on the early atmospheres of Earth, Venus and Mars. The main results of our study can be summarized as follows:

1) The early atmosphere of Earth about 4.0–4.5 Gyr ago may have had a Venus- or martian-like high content of CO_2, which is the most efficient IR-radiating cooler in planetary thermospheres, important to protect the upper atmosphere from high exobase temperatures and high loss rates.
2) An intrinsic planetary magnetic field like on present Earth, or early Mars is essential for the protection of an extended upper atmosphere from the XUV and solar wind induced erosion. An early martian dynamo larger than ∼0.1 $\mathcal{M}_e$ could reduce the ion erosion from the early martian atmosphere in an efficient way.

3) The modelled exobase temperatures obtained for early Earth, Venus and Mars after the young Sun arrived at the ZAMS indicate that periods of blow-off and diffusion-limited hydrodynamic escape of atomic hydrogen and high Jeans escape rates for heavier species like H_2, He, C, N, O, etc., should have occurred. The duration of this blow-off period for atomic hydrogen on each planet might essentially depend on the mixing ratios of CO_2, N_2, and H_2O in the atmosphere and could last from ∼100 to several hundred Myr.
4) Our model simulations show that atmospheric erosion by the solar wind ion pick up from a non-magnetized Venus could effectively erode O^+ ions during the first Gyr after the Sun arrived at the ZAMS. Depending on the solar wind parameters expected for the young Sun, an equivalent amount of up to one terrestrial ocean could be lost (see also Kulikov et al. 2006).

The comparative study of the early upper atmospheres of Earth, Venus, and Mars suggests that we will not be able to understand the evolution of Earth-type biospheres and habitability of terrestrial planets in general if we neglect atmospheric effects caused by the radiation and particle environment of the young Sun/stars, which change dramatically over the history of the solar/stellar system. Therefore, a better knowledge of early solar wind parameters including estimations of magnetic fields of young stellar systems and plasma outflow from young Sun-like stars is urgently needed. Thus, more projects/missions related to observations of solar proxies should be undertaken in the near future.

In conclusion we must also note that our findings presented in this study should be considered as preliminary and awaiting further confirmation of the hypotheses on which our reasoning is mainly based, and of the progress in relevant stellar and planetary observations and development of more advanced atmospheric loss models for analyzing observational data and making realistic predictions.

Acknowledgements The authors would like to thank Eric Chassefière and another anonymous reviewer for their constructive criticism of the manuscript and helpful suggestions. We also wish to thank the Editor, Kathryn Fishbaugh, for her valuable comments and recommendations. Yu.N. Kulikov, H. Lammer, H.I.M. Lichtenegger, T. Penz, and H.K. Biernat thank the "Österreichischer Austauschdienst" (ÖAD), which supported this work by the project I.12/04. The authors acknowledge also the support by the Austrian Academy of Sciences, "Verwaltungsstelle für Auslandsbeziehungen", by the Russian Academy of Sciences (RAS), for supporting working visits to the PGI/RAS in Murmansk, Russian Federation. Yu.N. Kulikov, H. Lammer and H.I.M. Lichtenegger also thank the Russian Foundation for the Basic Research, which supported this study as a joint Russian-Austrian project No. 03-05-20003 "Solar-planetary relations and space weather". H.K. Biernat and T. Penz also thanks the Austrian "Fonds zur Förderung der wissenschaftlichen Forschung" which supported this study under project P17099-N08. Yu.N. Kulikov, H. Lammer, and H.K. Biernat acknowledge also the International Space Science Institute (ISSI; Bern, Switzerland), as this study was partly carried out within the framework of the ISSI Team "Evolution of Habitable Planets".

References

M.H. Acuña et al., Science **279**, 1676–1680 (1998)
M.H. Acuña et al., Science **284**, 790–793 (1999)
U.V. Amerstorfer, H. Lammer, T. Tokano, F. Selsis, C. Kolb, A. Bérces, G. Kovács, M.R. Patel, C.S. Cockell, Gy. Rontó, T. Penz, N.V. Erkaev, H.K. Biernat, in *Proc. 3rd European Workshop on Exo/Astrobiology*, ed. by R.A. Harris, L. Ouwehand. ESA SP, vol. 545 (2004), pp. 165–166
T.R. Ayres, J. Geophys. Res. **102**, 1641–1651 (1997)
V.R. Baker, Nature **412**, 228–236 (2001)
J.L. Bandfield, T.D. Gloch, P.R. Christensen, Science **301**, 1084–1086 (2003)
S. Barabash, A. Fedorov, R. Lundin, J.-A. Sauvaud, Science **315**, 501–514 (2007)
C.A. Barth, A.I.F. Stewart, S.W. Bougher, D.M. Hunten, S.J. Bauer, A.F. Nagy, in *Mars* (Univ. Arizona Press, 1992), pp. 1054–1089

R.H. Becker, R.N. Clayton, E.M. Galimov, H. Lammer, B. Marty, R.O. Pepin, R. Weiler, Space Sci. Rev. **106**, 377–410 (2003)
J.-P. Biebring the OMEGA team, Science **307**, 1576–1581 (2005)
H.K. Biernat, N.V. Erkaev, C.J. Farrugia, Adv. Space Res. **28**, 833–839 (2001)
S.W. Bougher, G.M. Keating, Structure of the Mars Upper Atmosphere: MGS Aerobraking Data and Model Interpretation. The Fifth International Conference on Mars, July 19–24, 1999, Pasadena, California, abstract no. 6010, 1999
S.W. Bougher, S. Engel, R.G. Roble, B. Foster, J. Geophys. Res. **104**, 16,591–16,611 (1999)
S.W. Bougher, S. Engel, R.G. Roble, B. Foster, J. Geophys. Res. **105**, 17669–17692 (2000)
L.H. Brace, R.F. Theis, W.R. Hoegy, Planet. Space Sci. **30**, 29–37 (1982)
D.A. Brain, B.M. Jakosky, J. Geophys. Res. **103**, 22689–22694 (1998)
D. Breuer, T. Spohn, J. Geophys. Rev. **108**, 5072 (2003). doi: 10.1029/2002JE001999
F.H. Busse, Phys. Earth Planet. **12**, 350–358 (1976)
E. Carlsson, F. Fedorovc, S. Barabash, E. Budnik, A. Grigorieva, H. Gunell, H. Nilssona, J.-A. Sauvaud, R. Lundin, Y. Futaanaa, M. Holmström, H. Anderssona, M. Yamauchi, J.-D. Winningham, R.A. Frahmd, J.R. Sharber, J. Scherrer, A.J. Coates, D.R. Linder, D.O. Kataria, E. Kallio, H. Koskinen, T. Säles, P. Riihela, W. Schmidt, J. Kozyra, J. Luhmann, E. Roelof, D. Williams, S. Livi, C.C. Curtis, K.C. Hsiehj, B.R. Sandel, M. Grande, M. Carter, J.-J. Thocaven, S. McKenna-Lawlor, S. Orsini, R. Cerulli-Irelli, M. Maggi, P. Wurz, P. Bochsler, N. Krupp, J. Wocho, M. Fraenz, K. Asamura, C. Dierker, Icarus **182**, 320–328 (2006)
M.H. Carr, Nature **326**, 30–34 (1987)
J.W. Chamberlain, Planet. Space Sci. **11**, 901–996 (1963)
S. Chandra, A.K. Sinha, J. Geophys. Res. **79**, 1916–1921 (1974)
E. Chassefière, Icarus **124**, 537–552 (1996a)
E. Chassefière, J. Geophys. Res. **101**, 26039–26056 (1996b)
E. Chassefière, F. Leblanc, Planet. Space Sci. **52**, 1039–1058 (2004)
C.F. Chyba, P.J. Thomas, L. Brookshaw, C. Sagan, Science **249**, 366–373 (1990)
M. Cohen, L.V. Kuhi, Astrophys. J. Suppl. **41**, 743–843 (1979)
J.E.P. Connerney, M.H. Acuña, P. Wasilewski, N.F. Ness, H. Rème, C. Mazelle, D. Vignes, R.P. Lin, D. Mitchell, P. Cloutier, Science **284**, 794–798 (1999)
T.E. Cravens, J.U. Kozyra, A.F. Nagy, T.I. Gombosi, M. Kurtz, J. Geophys. Res. **92**, 7341–7353 (1987)
G. Crowley, Rev. Geophys. Suppl. **29**, 1143–1165 (1991)
M.O. Dayhoff, R. Eck, E.R. Lippincott, C. Sagan, Science **155**, 556–557 (1967)
V. Dehant, H. Lammer, Yu.N. Kulikov, J.-M. Grießmeier, D. Breuer, O. Verhoeven, Ö. Karatekin, T. van Hoolst, O. Korablev, P. Lognonné, Space Sci. Rev. (2007, this issue). doi: 10.1007/s11214-007-9163-9
R.E. Dickinson, J. Atmos. Sci. **29**, 1531–1556 (1972)
R.E. Dickinson, S.W. Bougher, J. Geophys. Res. **91**, 70–80 (1986)
R.E. Dickinson, R.G. Roble, S.W. Bougher, Adv. Space Res. **7**, (10)5–(10)15 (1987)
T. Donahue, J.H. Hoffman, A.J. Watson, Science **216**, 630–633 (1982)
T.M. Donahue, J.B. Pollack, in *Venus*, ed. by D.M. Hunten, L. Colin, T.M. Donahue, V.I. Moroz (University of Arizona Press, Tucson, 1983), pp. 1003–1036
T.M. Donahue, E. Hartle, Geophys. Res. Lett. **12**, 2449–2452 (1992)
J.D. Dorren, E.F. Guinan, in *The Sun as a Variable Star*, ed. by J.M. Pap, C. Frölich, H.S. Hudson, S.K. Solanki (Cambridge University Press, Cambridge, 1994), pp. 206–216
G. Dreibus, H. Wänke, Icarus **71**, 225–240 (1987)
F. Forget, R.T. Pierrehumbert, Science **278**, 1273–1276 (1997)
J.L. Fox, A. Dalgarno, J. Geophys. Res. **84**, 7315–7333 (1979)
J.L. Fox, A. Dalgarno, J. Geophys. Res. **86**, 629–639 (1981)
J.L. Fox, Planet. Space Sci. **36**, 37–46 (1988)
J.L. Fox, A. Hać, J. Geophys. Res. **102**, 24005–24011 (1997)
J.L. Fox, K.Y. Sung, J. Geophys. Res. **106**, 21305–21335 (2001)
J.L. Fox, F.M. Bakalian, J. Geophys. Res. **106**, 28785–28795 (2001)
J.-M. Grießmeier, U. Motschmann, A. Stadelmann, T. Penz, H. Lammer, F. Selsis, I. Ribas, E.F. Guinan, H.K. Biernat, W.W. Weiss, Astron. Astrophys. **425**, 753–762 (2004)
J.-M. Grießmeier, A. Stadelmann, U. Motschmann, N.K. Belisheva, H. Lammer, H.K. Biernat, Astrobiology **5**, 587–603 (2005)
G.V. Gridchin, E.A. Zhadin, A.I. Ivanovsky, V.A. Marchevsky, Geomagn. Aeron. **15**, 93–100 (1975)
D.H. Grinspoon, J.S. Lewis, Icarus **74**, 21–35 (1988)
S.H. Gross, J. Atmos. Sci. **29**, 214–218 (1972)
E.F. Guinan, I. Ribas, in *The Evolving Sun and Its Influence on Planetary Environments*, ed. by B. Montesinos, A. Giménz, E.F. Guinan. ASP, vol. 269 (San Francisco, 2002), pp. 85–107

B.F. Gordiets, M.N. Markov, L.A. Shelepin, Planet. Space Sci. **26**, 933–948 (1978)
B.F. Gordiets, Yu.N. Kulikov, M.N. Markov, M.Ya. Marov, Preprint FIAN, N 112 (1979)
B.F. Gordiets, Yu.N. Kulikov, Kosm. Issled. **19**, 249–260 (1981)
B.F. Gordiets, Yu.N. Kulikov, Kosm. Issled. **19**, 539–550 (1981)
B.F. Gordiets, Yu.N. Kulikov, Trudy FIAN **130**, 29–47 (1982)
B.F. Gordiets, Yu.N. Kulikov, M.N. Markov, M.Ya. Marov, J. Geophys. Res. **87**, 4504–4514 (1982)
B.F. Gordiets, A.I. Osipov, L.A. Shelepin, *Kinetic Processes in Gases and Molecular Lasers* (Nauka, Moscow, 1980), 512 pp. (English translation: Gordon and Breach, New York, 1987, 688 pp.)
B.F. Gordiets, Yu.N. Kulikov, Adv. Space Res. **5**, 113–117 (1985)
B.F. Gordiets, Trudy FIAN **212**, 109–122 (1991)
D.O. Gough, in *The Solar Output and Its Variations*, ed. by O.R. White (University of Colorado Press, Boulder, 1977), pp. 451–473
R.M. Haberle, D. Tyler, C.P. McKay, W.L. Davis, Icarus **109**, 102–120 (1994)
R.M. Haberle, J. Geophys. Res. **103**, 28467–28479 (1998)
W.B. Hanson, S. Santani, D.R. Zuccaro, J. Geophys. Res. **82**, 4351–4363 (1977)
R.E. Hartle, J.M. Grebowsky, J. Geophys. Res. **98**, 7437–7445 (1993)
R.E. Hartle, T.M. Donahue, J.M. Grebowsky, H.G. Mayr, J. Geophys. Res. **101**, 4525–4538 (1996)
W.K. Hartmann et al., in *Basaltic Volcanism on the Terrestrial Planets* (Pergamon, Tarrytown, 1981)
J.W. Head III, H. Hiesinger, M.A. Ivanov, M.A. Kreslavsky, S. Pratt, B.J. Thomson, Science **286**, 2134–2137 (1999)
A.E. Hedin, H.B. Nieman, W.T. Kasprzak, A. Seiff, J. Geophys. Res. **88**, 73–83 (1983)
A.M. Hessler, D.R. Lowe, R.L. Jones, D.K. Bird, Nature **428**, 736–738 (2004)
J.H. Hoffman, R.R. Hodges Jr., T.M. Donahue, M.B. McElroy, J. Geophys. Res. **85**, 7882–7890 (1980)
H.D. Holland, in *The Origin and Evolution of Atmospheres and Oceans*, ed. by P.J. Brancasio, A.G.W. Cameron (Wiley, New York, 1963), pp. 86–101
D.J. Hollenbach, S.S. Prasad, R.C. Witten, Icarus **64**, 205–220 (1985)
D.M. Hunten, T.M. Donahue, J.C.G. Walker, J.F. Kasting, in *Origin and Evolution of Planetary and Satellite Atmospheres*, ed. by S.K. Atreya, J.B. Pollack, M.S. Matthews (University of Arizona Press, Tucson, 1987), pp. 386–423
D.M. Hunten, Science **259**, 915–920 (1993)
K.S. Hutchins, B.M. Jakosky, J.G. Luhmann, J. Geophys. Res. **102**, 9183–9189 (1997)
W.-H. Ip, Icarus **76**, 135–145 (1988)
I. Iben Jr., Astrophys. J. **141**, 993–1018 (1965)
M.N. Izakov, Space Sci. Rev. **12**, 261–298 (1971)
L.G. Jacchia, Thermospheric temperature, density and composition: New models. Spec. Rep., 375, Smithson. Inst. Astrophys. Obs., Cambridge, 1977
B.M. Jakosky, R.O. Pepin, R.E. Johnson, J.L. Fox, Icarus **111**, 271–288 (1994)
J.H. Jeans, *The Dynamical Theory of Gases*, 4th edn. (Cambridge University Press, Cambridge, 1925)
R.E. Johnson, M. Liu, J. Geophys. Res. **101**, 3649–3647 (1996)
N.M. Johnson, B. Fegley, Icarus **146**, 301–306 (2000)
R.E. Johnson, D. Schnellenberger, M.C. Wong, J. Geophys. Res. **105**, 1659–1670 (2000)
E. Kallio, J.G. Luhmann, S. Barabash, J. Geophys. Res. **102**, 22183–22197 (1997)
E. Kallio, P. Janhunen, Annales Geophysicae **21**, 2133–2145 (2003)
D.M. Kass, Y.L. Yung, Science **268**, 697–699 (1995)
D.M. Kass, Y.L. Yung, Science **274**, 1932–1933 (1996)
J.F. Kasting, J.B. Pollack, Icarus **53**, 479–508 (1983)
J.F. Kasting, J.B. Pollack, T.P. Ackerman, Icarus **57**, 335–355 (1984)
J.F. Kasting, Icarus **74**, 472–494 (1988)
J.F. Kasting, Icarus **94**, 1–13 (1991)
G.M. Keating, R.H. Tolson, T.J. Schellenberg, N.C. Hsu, S.W. Bougher, Study of Venus upper atmosphere using Magellan drag measurements. Second Ann. Progress Rep., NAG5-6081, NASA, Washington DC, 1998
J. Kim, A.F. Nagy, J.L. Fox, T. Craven, J. Geophys. Res. **103**, 29,339–29,342 (1998)
Yu.N. Kulikov, H. Lammer, H.I.M. Lichtenegger, N. Terada, I. Ribas, C. Kolb, D. Langmayr, R. Lundin, E.F. Guinan, S. Barabash, H.K. Biernat, Planet. Space Sci. **54**, 1425–1444 (2006)
H. Lammer, S.J. Bauer, J. Geophys. Res. **96**, 1819–1825 (1991)
H. Lammer, W. Stumptner, G.-J. Molina-Cuberos, S.J. Bauer, T. Owen, Planet. Space Sci. **48**, 529–543 (2000a)
H. Lammer, W. Stumptner, S.J. Bauer, Planet. Space Sci. **48**, 1473–1478 (2000b)
H. Lammer, S.J. Bauer, Space Sci. Rev. **106**, 281–292 (2003)

H. Lammer, H.I.M. Lichtenegger, C. Kolb, I. Ribas, E.F. Guinan, R. Abart, S.J. Bauer, Icarus **106**, 9–25 (2003a)
H. Lammer, C. Kolb, T. Penz, U.V. Amerstorfer, H.K. Biernat, B. Bodiselitsch, Int. J. Astrobiol. **2**, 1–8 (2003b)
H. Lammer, H.I.M. Lichtenegger, H.K. Biernat, N.V. Erkaev, I.L. Arshukova, C. Kolb, H. Gunell, A. Lukyanov, M. Holmstrom, S. Barabash, T.L. Zhang, W. Baumjohann, Planet. Space Sci. **54**, 1445–1456 (2006)
F. Leblanc, R.E. Johnson, Planet. Space Sci. **49**, 645–656 (2001)
F. Leblanc, R.E. Johnson, J. Geophys. Res. **107**, 1–6 (2002)
J.S. Lewis, Earth Planet. Sci. Lett. **10**, 73–80 (1970)
J.S. Lewis, Icarus **16**, 241–252 (1972)
J.S. Lewis, Space Sci. Rev. **14**, 401–410 (1973)
J.S. Lewis, Science **186**, 440–443 (1974)
J.S. Lewis, R.G. Prinn, *Planets and Their Atmospheres: Origin and Evolution* (Academic, New York, 1984)
H.I.M. Lichtenegger, E.M. Dubinin, Earth Planets Space **50**, 445–452 (1998)
H.I.M. Lichtenegger, H. Lammer, W. Stumptner, J. Geophys. Res. **107**, 1279 (2002). doi: 10.1029/2001JA000322
J.G. Luhmann, J.U. Kozyra, J. Geophys. Res. **96**, 5457–5467 (1991)
J.G. Luhmann, R.E. Johnson, M.G.H. Zhang, Geophys. Res. Lett. **19**, 2151–2154 (1992)
J.G. Luhmann, J. Geophys. Res. **98**, 17615–17621 (1993)
J.G. Luhmann, J. Geophys. Res. **102**, 1637 (1997)
R. Lundin, A. Zakharov, R. Pellinen, B. Hultquist, H. Borg, E.M. Dubinin, S. Barabash, N. Pissarenko, H. Koskinnen, I. Liede, Nature **341**, 609–612 (1989)
R. Lundin, A. Zakharov, R. Pellinen, S.W. Barabash, H. Borg, E.M. Dubinin, B. Hultquist, H. Koskinen, I. Liede, N. Pissarenko, Geophys. Res. Lett. **17**, 873–876 (1990)
R. Lundin, E.M. Dubinin, H. Koskinen, O. Norberg, N. Pissarenko, S.W. Barabash, Geophys. Res. Lett. **18**, 1059–1062 (1991)
R. Lundin et al., Science **305**, 1933–1936 (2004)
R. Lundin, H. Lammer, I. Ribas, Space Sci. Rev. (2007, this issue). doi: 10.1007/s11214-007-9176-4
J.A. Magalhaes, J.T. Schofield, A. Seiff, J. Geophys. Res. **104**, 8943–8955 (1999)
C.V. Manning, C.P. McKay, K.J. Zahnle, Icarus **180**, 38–59 (2006)
P. McKay, C.R. Stocker, Rev. Geophys. **27**, 189–214 (1989)
M.T. Mellon, Icarus **124**, 268–279 (1996)
H.J. Melosh, A. Vickery, Nature **338**, 487–489 (1989)
M.B. McElroy, M.J. Prather, J.M. Rodriguez, Science **215**, 1614–1615 (1982)
A. Morbidelli, J. Chambers, J.I. Lunine, J.M. Petit, F. Robert, G.B. Valsecchi, K. Cyr, Meteorit. Planet. Sci. **35**, 1309–1320 (2000)
V.I. Moroz, N.A. Parfentev, N.F. Sanko, Kosm. Issled. **17**, 727–742 (1979)
A.F. Nagy, T.E. Cravens, J.H. Yee, A.I.F. Stewart, Geophys. Res. Lett. **8**, 629–632 (1981)
A.F. Nagy, J. Kim, T.E. Cravens, Ann. Geophys. **8**, 251–256 (1990)
H.B. Nieman, R.E. Hartle, W.T. Kasprzak, N.W. Spencer, D.M. Hunten, G.R. Carignan, Science **203**, 770–772 (1979a)
H.B. Nieman, R.E. Hartle, A.E. Hedin, W.T. Kasprzak, N.W. Spencer, D.M. Hunten, G.R. Carignan, Science **205**, 54–56 (1979b)
H.B. Niemann, W.T. Kasprzak, A.E. Hedin, D.M. Hunten, W. Spencer, J. Geophys. Res. **85**, 7817–7827 (1980)
A.O. Nier, M.B. McElroy, J. Geophys. Res. **82**, 4341–4349 (1977)
G. Newkirk Jr., Geochim. Cosmochim. Acta Suppl. **13**, 293–301 (1980)
M. Ozima, K. Seki, N. Terada, Y.N. Miura, F.A. Podosek, H. Shinagawa, Nature **436**, 655–659 (2005)
E.J. Öpik, Geophys. J. Roy. Astron. Soc. **7**, 490–526 (1963)
T. Penz, N.V. Erkaev, H.K. Biernat, H. Lammer, U.V. Amerstorfer, H. Gunell, E. Kallio, S. Barabash, S. Orsini, A. Milillo, W. Baumjohann, Planet. Space Sci. **52**, 1157–1167 (2004)
R.O. Pepin, Icarus **111**, 289–304 (1994)
J.B. Pollack, Icarus **14**, 295–306 (1971)
S.I. Rasool, C. De Bergh, Nature **226**, 1037–1039 (1970)
R. Raye, O. Kuo, H.D. Holland, Nature **378**, 603–605 (1995)
S.N. Raymond, T. Quinn, J.I. Lunine, Icarus **168**, 1–17 (2004)
I. Ribas, E.F. Guinan, M. Güdel, M. Audard, Astrophys. J. **622**, 680–694 (2005)
P.G. Richards, D.G. Torr, J. Geophys. Res. **93**, 4060–4066 (1988)
J.M. Rodriguez, M.J. Prather, M.B. McElroy, Planet. Space Sci. **32**, 1235–1255 (1984)
J. Rosenqvist, E. Chassefière, Planet. Space Sci. **43**, 3–10 (1995)

C.T. Russell, J.G. Luhmann, R.C. Elphic, F.L. Scarf, L.H. Brace, Geophys. Res. Lett. **9**, 45–48 (1982)
J.T. Schofield et al., Science **278**, 1752–1758 (1997)
G. Schubert, T. Spohn, J. Geophys. Res. **95**, 14095–14104 (1990)
G. Schubert, C.T. Russell, W.B. Moore, Nature **408**, 666–667 (2000)
Y. Shimazu, T. Urabe, Icarus **9**, 498–506 (1968)
H. Shinagawa, T.E. Cravens, A.F. Nagy, J. Geophys. Res. **92**, 7317–7330 (1987)
R.W. Shunk, A.F. Nagy, *Ionospheres – Physics, Plasma Physics, and Chemistry* (Cambridge University Press, Cambridge, 2000)
J.A. Slavin, R.E. Holzer, J. Geophys. Res. **84**, 2076–2082 (1979)
N.H. Sleep, J. Geophys. Res. **99**, 5639–5655 (1994)
J.R. Spreiter, NASA Spec. Publ. **SP-397**, 135–149 (1975)
J.R. Spreiter, S.S. Stahara, J. Geophys. Res. **98**, 17,251–17,262 (1980)
S.W. Squyres, J.F. Kasting, Science **265**, 744–748 (1994)
D.J. Stevenson, T. Spohn, G. Schubert, Icarus **54**, 466–489 (1983)
C.P. Sonnett, M.S. Giampapa, M.S. Matthews, *The Sun in Time* (University of Arizona Press, Tucson, 1991)
N. Terada, S. Machida, H. Shinagawa, J. Geophys. Res. **107**, 1471–1490 (2002). doi: 10.1029/2001JA009224
F. Tian, O.B. Toon, A.A. Pavlov, H. De Sterck, Science **308**, 1014–1017 (2005)
F. Tian, O.B. Toon, A.A. Pavlov, Science **311**, 38b (2006)
D.G. Torr, M.R. Torr, J. Atmos. Terr. Phys. **41**, 799–839 (1979)
M.R. Torr, P.G. Richards, D.G. Torr, J. Geophys. Res. **85**, 6819–6826 (1980)
A. Vidal-Madjar, A. Lecavelier des Etangs, J.-M. Désert, G.E. Ballester, R. Ferlet, G. Hébrard, M. Mayor, Nature **422**, 143–146 (2003)
U. Von Zahn, K.H. Fricke, D.M. Hunten, D. Krankowsky, K. Mauersberger, A.O. Nier, J. Geophys. Res. **85**, 7829–7840 (1980)
J.C.G. Walker, J. Atmos. Sci. **32**, 1248–1256 (1975)
H. Wänke, G. Dreibus, Philos. Trans. Roy. Soc. London Ser. A. **349**, 285–293 (1994)
B.P. Weiss, H. Vali, F.J. Baudenbacher, J.L. Kirschvink, S.T. Stewart, D.L. Shuster, Earth Planet. Sci. Lett. **201**, 449–463 (2002)
G.W. Wetherill, Icarus **46**, 70–80 (1981)
B.E. Wood, H.-R. Müller, G. Zank, J.L. Linsky, Astrophys. J. **574**, 412–425 (2002)
B.E. Wood, H.-R. Müller, G.P. Zank, J.L. Linsky, S. Redfield, Astrophys. J. **628**, L143–L146 (2005)
R. Yelle, Icarus **170**, 167–179 (2004)
K.J. Zahnle, J.C.G. Walker, Rev. Geophys. **20**, 280–292 (1982)
K. Zahnle, J.B. Pollack, J.F. Kasting, Icarus **84**, 503–527 (1990)
A.P. Zent, R.C. Quinn, J. Geophys. Res. **100**, 5341–5349 (1995)
M.H.G. Zhang, J.G. Luhmann, S.W. Bougher, A.F. Nagy, J. Geophys. Res. **98**, 10,915–10,923 (1993a)
M.H.G. Zhang, J.G. Luhmann, A.F. Nagy, J.S. Spreiter, S.S. Stahara, J. Geophys. Res. **98**, 3311–3318 (1993b)